99 7/16/79

dr. 2429

ANL-79-2

MASTER

ANL-79-2

MATERIALS TECHNOLOGY FOR COAL-CONVERSION PROCESSES

Fifteenth Quarterly Report, July—September 1978

U of C-AUA-USDOE

ARGONNE NATIONAL LABORATORY, ARGONNE, ILLINOIS

Prepared for the Office of Fossil Energy,
U. S. DEPARTMENT OF ENERGY
under Contract W-31-109-Eng-38

DISTRIBUTION OF THIS DOCUMENT IS UNLIMITED

DISCLAIMER

This report was prepared as an account of work sponsored by an agency of the United States Government. Neither the United States Government nor any agency Thereof, nor any of their employees, makes any warranty, express or implied, or assumes any legal liability or responsibility for the accuracy, completeness, or usefulness of any information, apparatus, product, or process disclosed, or represents that its use would not infringe privately owned rights. Reference herein to any specific commercial product, process, or service by trade name, trademark, manufacturer, or otherwise does not necessarily constitute or imply its endorsement, recommendation, or favoring by the United States Government or any agency thereof. The views and opinions of authors expressed herein do not necessarily state or reflect those of the United States Government or any agency thereof.

DISCLAIMER

Portions of this document may be illegible in electronic image products. Images are produced from the best available original document.

The facilities of Argonne National Laboratory are owned by the United States Government. Under the terms of a contract (W-31-109-Eng-38) between the U. S. Department of Energy, Argonne Universities Association and The University of Chicago, the University employs the staff and operates the Laboratory in accordance with policies and programs formulated, approved and reviewed by the Association.

MEMBERS OF ARGONNE UNIVERSITIES ASSOCIATION

The University of Arizona
Carnegie-Mellon University
Case Western Reserve University
The University of Chicago
University of Cincinnati
Illinois Institute of Technology
University of Illinois
Indiana University
Iowa State University
The University of Iowa
Kansas State University
The University of Kansas
Loyola University
Marquette University
Michigan State University
The University of Michigan
University of Minnesota
University of Missouri
Northwestern University
University of Notre Dame
The Ohio State University
Ohio University
The Pennsylvania State University
Purdue University
Saint Louis University
Southern Illinois University
The University of Texas at Austin
Washington University
Wayne State University
The University of Wisconsin

NOTICE

This report was prepared as an account of work sponsored by the United States Government. Neither the United States nor the United States Department of Energy, nor any of their employees, nor any of their contractors, subcontractors, or their employees, makes any warranty, express or implied, or assumes any legal liability or responsibility for the accuracy, completeness or usefulness of any information, apparatus, product or process disclosed, or represents that its use would not infringe privately-owned rights. Mention of commercial products, their manufacturers, or their suppliers in this publication does not imply or connote approval or disapproval of the product by Argonne National Laboratory or the U. S. Department of Energy.

Printed in the United States of America
Available from
National Technical Information Service
U. S. Department of Commerce
5285 Port Royal Road
Springfield, Virginia 22161
Price: Printed Copy $5.25; Microfiche $3.00

Distribution Category:
Coal Conversion and Utilization--
Coal Gasification (UC-90c)

ANL-79-2

ARGONNE NATIONAL LABORATORY
9700 South Cass Avenue
Argonne, Illinois 60439

MATERIALS TECHNOLOGY FOR COAL-CONVERSION PROCESSES

Fifteenth Quarterly Report, July—September 1978

W. A. Ellingson
Project Leader

Materials Science Division

NOTICE

This report was prepared as an account of work sponsored by the United States Government. Neither the United States nor the United States Department of Energy, nor any of their employees, nor any of their contractors, subcontractors, or their employees, makes any warranty, express or implied, or assumes any legal liability or responsibility for the accuracy, completeness or usefulness of any information, apparatus, product or process disclosed, or represents that its use would not infringe privately owned rights.

Previous reports in this series

ANL-77-62	April—June 1977
ANL-78-6	July—December 1977
ANL-78-54	January—March 1978
ANL-78-79	April—June 1978

DISTRIBUTION OF THIS DOCUMENT IS UNLIMITED

THIS PAGE
WAS INTENTIONALLY
LEFT BLANK

TABLE OF CONTENTS

LIST OF FIGURES

LIST OF FIGURES (contd.)

LIST OF TABLES

MATERIALS TECHNOLOGY FOR COAL-CONVERSION PROCESSES: FIFTEENTH QUARTERLY REPORT,
July-September 1978

HIGHLIGHTS

Task A -- Evaluation of Ceramic Refractories for Slagging Gasifiers
(C.R. Kennedy, D.J. Jones, R.J. Fousek, and R.B. Poeppel)

The results from test run 9 have been compiled and analyzed. Although the slag was basic as formulated, chemical analyses revealed that the slag was acidic for $\gtrsim$ 98% of the test (probably as a result of formation of precipitates in the slag pool).

The fused-cast chrome-spinel refractory (number 22) exhibited excellent corrosion resistance at $\sim$ 1550°C, even without water cooling. The fused-cast chrome-alumina (number 38) also performed well, whereas the silicon carbide and alumina-silica refractories exhibited substantial corrosion.

Task C -- Application and Development of Nondestructive Evaluation Methods for Coal-conversion Processes
(W.A. Ellingson, K.J. Reimann, W.J. Shack, and C.A. Youngdahl)

Field work on ultrasonic erosion-detection systems has continued with data acquisition during a plant run at Bi-Gas. The work on ultrasonic measurement of surface roughness has been advanced this quarter through receipt and check-out of a hard disk drive system for the minicomputer. A third large cast-refractory test panel was heated and air quenched. Preliminary results show that maximum acoustic output again occurred during rapid heating. In studies on a 6-in. high-pressure valve, an initial linear correlation has been obtained between a differential-pressure system and the acoustic valve-leak detection system.

Task D.1 -- Corrosion in Gasification Environments
(K. Natesan)

Uniaxial tensile data were generated for Incoloy 800, Type 310 stainless steel, Inconel 671, and U.S. Steel Alloy 18-18-2 after a 3.6-Ms exposure to multicomponent gas mixtures that simulate a coal-gasification environment. The preexposure of the materials to complex gas mixtures resulted in a decrease in ultimate tensile strength with only minimal changes in the uniform strain over the range of $\sim$ 4 to 13%. The decrease in strength properties was more pronounced when the oxygen partial pressure in the gas mixture was lower.

Task D.2 -- Corrosion in Atmospheric Fluidized-bed Environments
(O.K. Chopra)

The effects of NaCl and $CaCl_2$ additions on the corrosion behavior of materials in a fluidized-bed environment have been evaluated. The corrosive attack consisted primarily of oxidation with some degree of sulfidation at temperatures between 723 and 1123 K. Iron-base alloys, e.g., Types 304, 316 and 310 stainless steel, exhibited greater corrosion resistance than materials with high nickel content, e.g. RA333 and Inconel 600 and 601. The addition of slag to the fluidized bed increased the corrosive attack on all materials.

Task E -- Erosion Behavior of Materials in Coal-conversion Processes
(J.Y. Park, S. Danyluk, and W.J. Shack)

Work has continued on the refurbishing and calibration of the high-temperature erosion-test apparatus. The particle-feeding, environmental control and heating systems have been installed. High-temperature corrosion calibration tests will begin next quarter.

Task F -- Component Performance and Failure Analysis *(S. Danyluk, G.M. Dragel, C.A. Youngdahl and L. Pahis)*

Block valves from the Liquid Phase Methanation (LPM) plant at HYGAS and the microstructure of piping from the HYGAS pilot plant were examined to determine whether a fire that had occurred at the LPM plant had adversely affected the structural components of the plant. A visit was made to HYGAS to examine cracks in the reactor cover plate. Offgas piping from HYGAS was analyzed to determine the nature of leaking cracks that were discovered near welds.

MATERIALS TECHNOLOGY FOR COAL-CONVERSION PROCESSES: FIFTEENTH QUARTERLY REPORT, July-September 1978

ABSTRACT

This broad-base materials engineering program, begun in 1974, includes studies on ceramic (refractory) and metallic materials presently being used or intended for use in coal-conversion processes. The program entails studies of erosive wear, nondestructive testing, corrosion, refractory degradation, and failure analysis. Appropriate laboratory and field experiments are integrated such that the results have impact on present pilot- and demonstration-plant and proposed full-scale designs. This quarterly report, for the period July-September 1978, presents the technical accomplishments of the program.

INTRODUCTION

The economical conversion of coal into clean and usable fuels will be advanced through the use of durable materials systems. The technical information base required for materials selection in plant design for the operating environments of various coal-conversion processes is extremely limited. Hence, reliable selection and lifetime-prediction methods for materials under these conditions are not available. This project is designed to provide part of the materials information necessary for successful operation of coal-conversion systems. The present report is the fifteenth quarterly progress report submitted by ANL to the Division of System Engineering, Office of Fossil Energy under project Number 7106, "Materials Technology for Coal Conversion Processes".

The project includes six tasks: (A) evaluation of commercial refractories exposed to coal slag under conditions typical of those encountered in slagging gasification processes; (B) evaluation of erosion/corrosion-resistant coatings when exposed to prototype operating environments (temporarily discontinued in FY 78); (C) development, evaluation, and application of nondestructive evaluation methods applicable to coal-conversion systems; (D) evaluation of the corrosion behavior of commercial alloys; (E) development of analytical models with experimental verification for the prediction of erosive-wear behavior of materials used in coal-conversion plants; and (F) analysis of failed coal-conversion plant components.

Task A -- Evaluation of Ceramic Refractories for Slagging Gasifiers

(C. R. Kennedy, D. J. Jones, R. J. Fousek, and R. B. Poeppel)

The results from test run 9 have been compiled and analyzed. Included in this test were a chrome-spinel (number 22), a chrome-alumina (number 38), an alumina-silica (number 14), and three silicon carbide (numbers 37, 91, and 93) refractories. The compositions of these bricks are shown in Table I. Water-cooled 1/2-length and full-length [229-mm (9-in.)] samples of numbers 22, 38, 91, 93, and 14, a water-cooled 1/2-length sample of number 37, and an uncooled 1/2-length sample of refractory number 22 were exposed to a simulated North Dakota Lignite slag with an initial base-to-acid ratio of 1.7 (Table II). Also included in the center of the slag bath was an uncooled standard specimen (115 x 64 x 54 mm) of refractory number 2 (a fused-cast alumina).

Slag was added to a depth of $\sim$50 mm ($\sim$2 in.) and the furnace plenum temperature was held at 1540-1590°C for 455 h. An additional $\sim$25 mm ($\sim$1 in.) of slag was then put in and the furnace plenum temperature was maintained at $\sim$1480-1530°C for 474 more hours. The complete temperature history is shown in Fig. 1. Note that in addition to the plenum temperature and the temperatures 38 mm from the hot face, the hot-face temperature of the full-size number 14 brick was measured. The thermal gradients that existed within the bricks at 120 h into the test are shown in Fig. 2. The partial pressure of oxygen was maintained at about 10^{-3} Pa throughout the test.

The slag composition as a function of time is shown in Table II. Although the slag was basic (B/A = 1.7) as formulated, a chemical analysis of a sample taken just seven hours after the initial charge showed that the slag was acidic (B/A = 0.8), like the simulated Montana Rosebud in runs 4-8. As shown in Table II, the slag chemistry was actually acidic for $\gtrsim$98% of the test. This is probably the result of crystallization that occurred on the bottom of the slag bath, and is currently being investigated. From visual observations, the rotational velocity of the slag bath (induced by the tangential firing of the burners) was estimated to be $\sim$8-12 mm/s ($\sim$1/3-1/2 in./s) at a plenum temperature of 1580°C.

The relative corrosion resistance of the refractories exposed to slag attack in test run 9 is shown in Table I. As early as 94 h into the test, deep cuts at the slag line were evident in refractories number 14 and 91, as well as the standard specimen in the center of the bath (note that these were the only three refractories that could be seen through the viewport). At some time between 94 and 142 h, the standard specimen was completely eaten through at the slag line. Two lines of slag attack are clearly visible on cut sections of certain refractories (Fig. 3). Comparison of the corrosion rate for the alumina-silica refractory (number 14) in test run 9 with the rates obtained for this same refractory in other acidic slag tests (see Table III) confirms that this was a severe test. Nevertheless, the chrome-spinel and alumina-chrome refractories exhibited little corrosion. Even without water cooling, the 1/2-length chrome-spinel brick (number 22) suffered only 2 mm of attack after 475 h at $\sim$1550°C. Thermal-shock cracking was evident in the water-cooled chrome-spinel and alumina-chrome refractories, but not in the uncooled

1/2-length chrome-spinel brick.

All three types of silicon carbide performed poorly, in contrast to the results obtained at a slightly lower temperature in test run 4. This indicates that at hot-face temperatures of $\gtrsim$1425°C, corrosion occurs very quickly. Although the exact mechanism is not clear at this time, large quantities of metal were found at the slag-refractory interface. This observation, along with the occurrence of many voids in the slag emanating from the reaction zone (clearly visible near the bottom attack line in Figs. 3e-3g), suggests that iron oxides reacted with the silicon carbide grain to form a ferrosilicon alloy and a CO/CO_2 gas (which was trapped after the second addition of slag).

TABLE I. Relative Corrosion Resistance of Water-cooled Refractories Exposed to Slag Attack in Test Run 9

Refractory Number	Composition	Type	Attack Line	Maximum Depth of Removal,[a] mm	
				Full-length	1/2-length
38	$Al_2O_3(60)-Cr_2O_3(27)-MgO(6)-Fe_2O_3(4)-SiO_2(2)$	Fused-cast	Top	4	2
			Bottom	3	2
22	$Cr_2O_3(80)-MgO(8)-Fe_2O_3(6)-Al_2C_3(5)-SiO_2(1)$	Fused-cast	Top	1	~ 0
			Bottom	1	~ 0.5
			Top[b]	-	2
			Bottom[b]	-	2
91	$SiC(75)-Si_3N_4(23)$	Sintered	Top	14	12
			Bottom	38	31
93	$SiC(73)-Al_2O_3(14)-SiO_2(11)$	Sintered	Top	14	12
			Bottom	36	28
37	$SiC(90)-Si_2ON_2(9)$	Sintered	Top	-	13
			Bottom	-	32
14	$Al_2O_3(91.6)-SiO_2(8.0)-Fe_2O_3(0.15)-Alkali(0.15)$	Sintered	Top	22	24
			Bottom	46	35

[a] Measured from the original hot face.

[b] Without water cooling.

TABLE II. Composition of Slag (wt %) during Corrosion Test Run 9

Component	Exposure Time, h 0	7	95	345	430	470	676	920
SiO_2 (S)	24.3	35.2	40.0	40.1	39.7	35.0	39.6	41.0
Al_2O_3 (A)	12.9	21.3	20.3	16.7	17.7	16.2	17.2	16.9
Fe_2O_3 (F_1)	11.4	1.1	0.9	2.1	1.3	1.8	1.9	2.2
FeO (F_2)	0	5.0	1.8	4.5	2.1	4.7	3.7	3.8
Fe (F_3)	0	0.5	0.4	0.4	0.4	0.4	0.3	0.4
CaO (C)	33.8	27.3	28.0	27.3	30.0	31.1	28.6	27.4
MgO (M)	9.7	7.0	6.7	6.6	6.7	7.8	7.1	6.8
Na_2O (N)	4.2	1.4	0.9	0.9	1.0	1.5	0.5	0.5
K_2O (K)	3.1	0.6	0.4	0.4	0.4	0.9	0.2	0.1
TiO_2 (T)	0.6	0.6	0.6	0.7	0.7	0.6	0.7	0.7
Other	0	0	0	0.3	0	0	0.2	0.2
B/A Ratio[a]	1.7	0.8	0.6	0.7	0.8	0.9	0.7	0.7
Ferritic Content,[b] %	100	15	26	27	31	24	30	31

[a] Base-to-acid ratio $B/A = (F_1 + F_2 + F_3 + C + M + N + K)/(S + A + T)$.

[b] $$\text{Ferritic content} = \frac{\text{wt \% } Fe_2O_3}{\text{wt \% } Fe_2O_3 + 1.11 \text{ wt \% FeO} + 1.43 \text{ wt \% Fe}} .$$

TABLE III. Corrosion Rate of an Alumina-Silica Refractory (Number 14) in Contact with an Acidic Slag as a Function of Temperature

Test Run No.	Plenum Temperature, °C	Water Cooling	Hot Face Temperature, °C	Average Attack Rate, mm/h
1	~1500	No	~1470	6.0×10^{-2}
7	1480-1520	Yes	1380-1420	1.9×10^{-2}
9[a]	1480-1530	Yes	1400-1440	4.7×10^{-2}
9[b]	1540-1590	Yes	1460-1510	10.1×10^{-2}

[a] Top attack line.

[b] Bottom attack line.

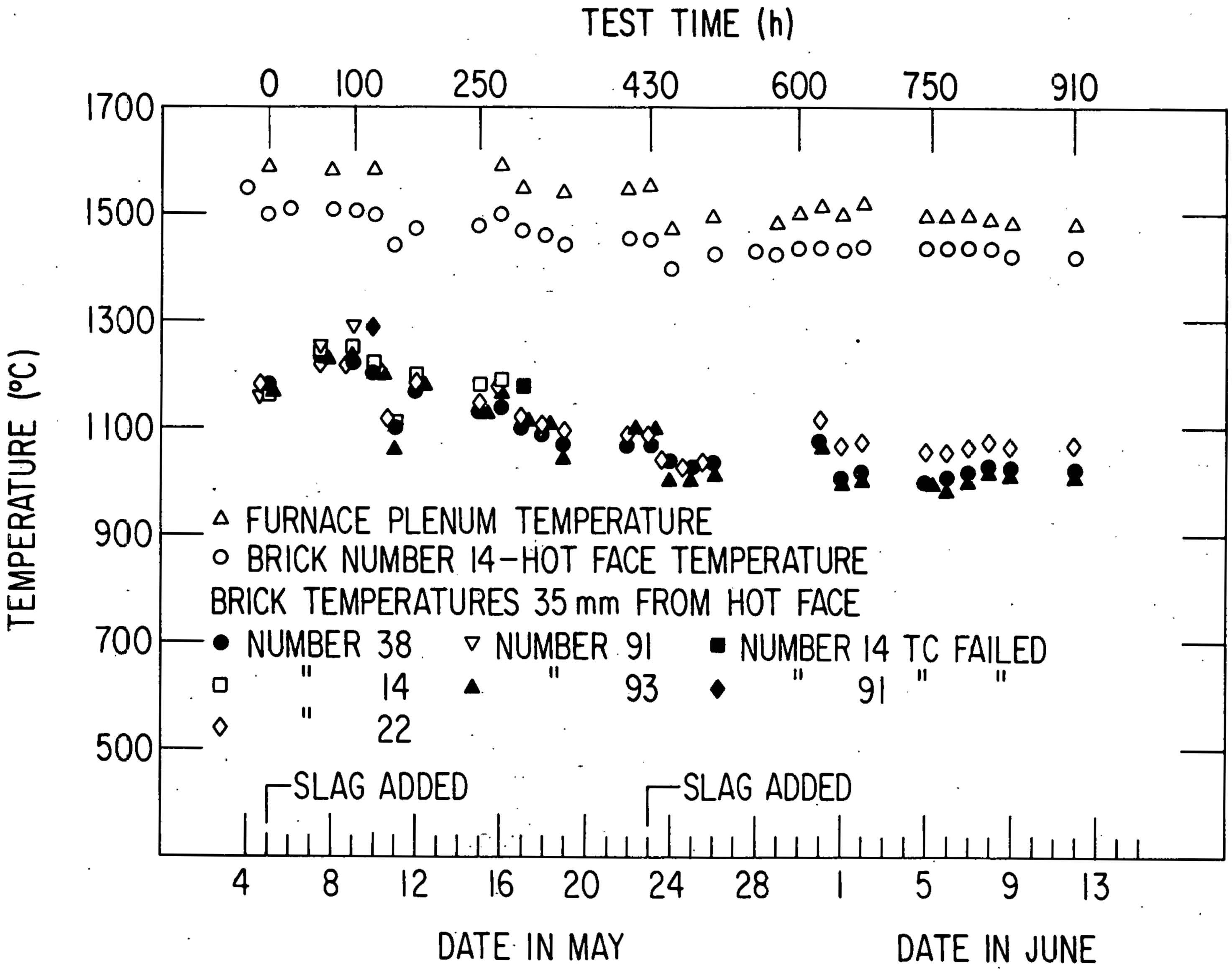

Fig. 1. Furnace Plenum Temperatures and Midheight Brick Temperatures 38 mm (1.5 in.) from the Hot Face of Full-size Bricks of Each Composition During Test Run 9. ANL Neg. No. 306-78-923.

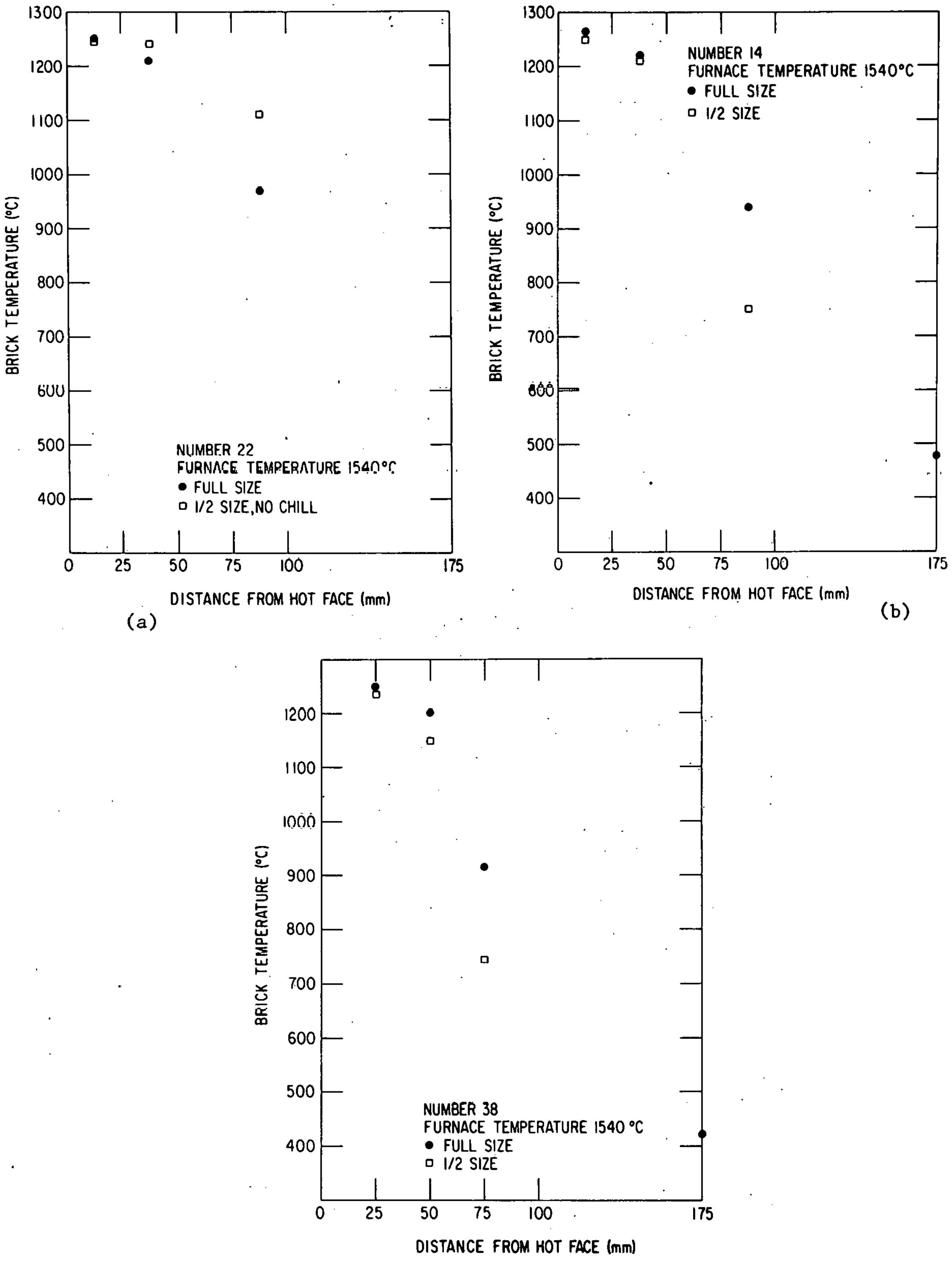

(a)

(b)

(c)

Fig. 2. Brick Temperature at Midheight Versus Distance from Hot Face. (a) Number 22, (b) number 14, (c) number 38, (d) number 91, (e) number 93, and (f) number 37. ANL Neg. Nos. 306-78-925, 924.

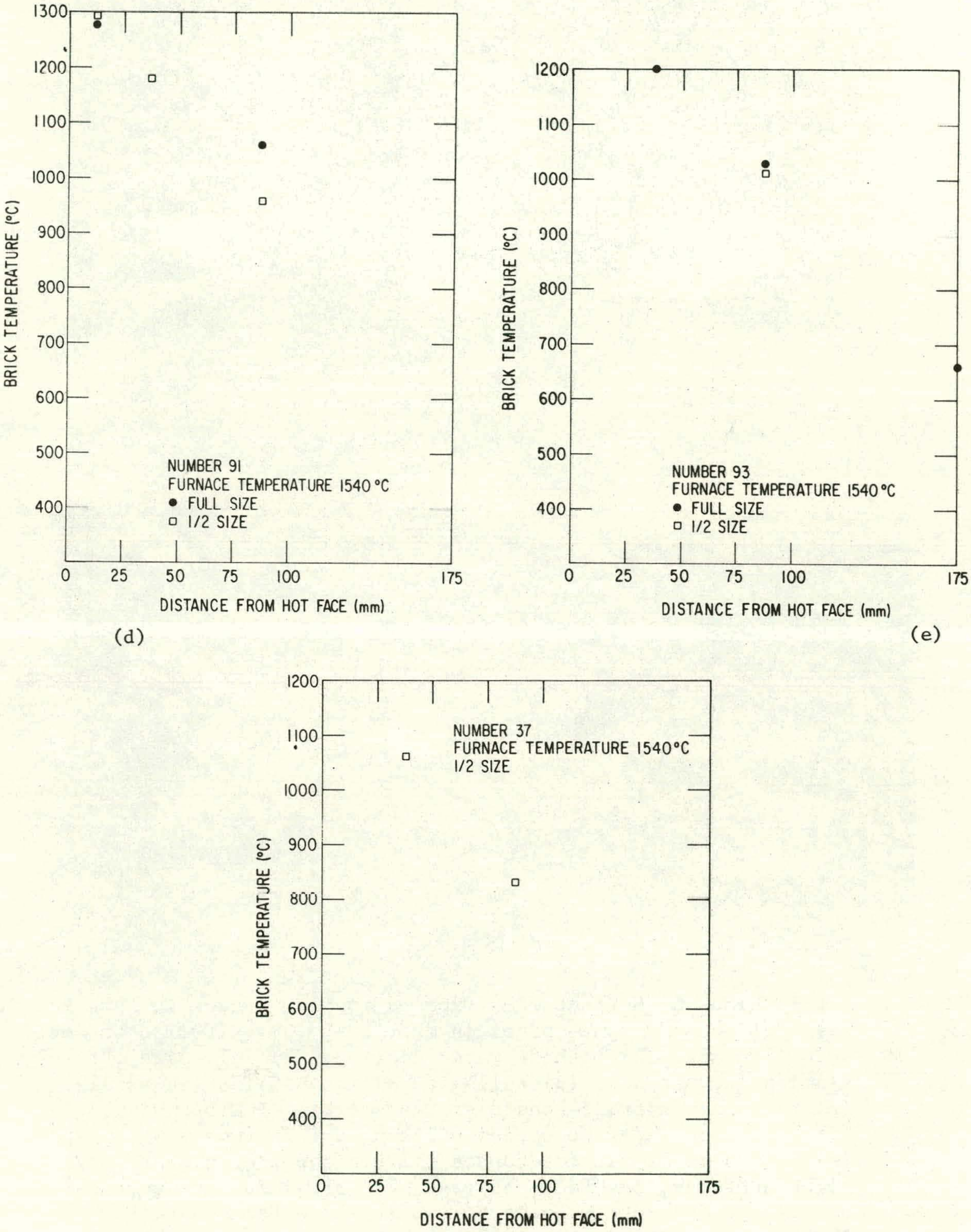

(d)

(e)

(f)

Fig. 2. (Contd.)

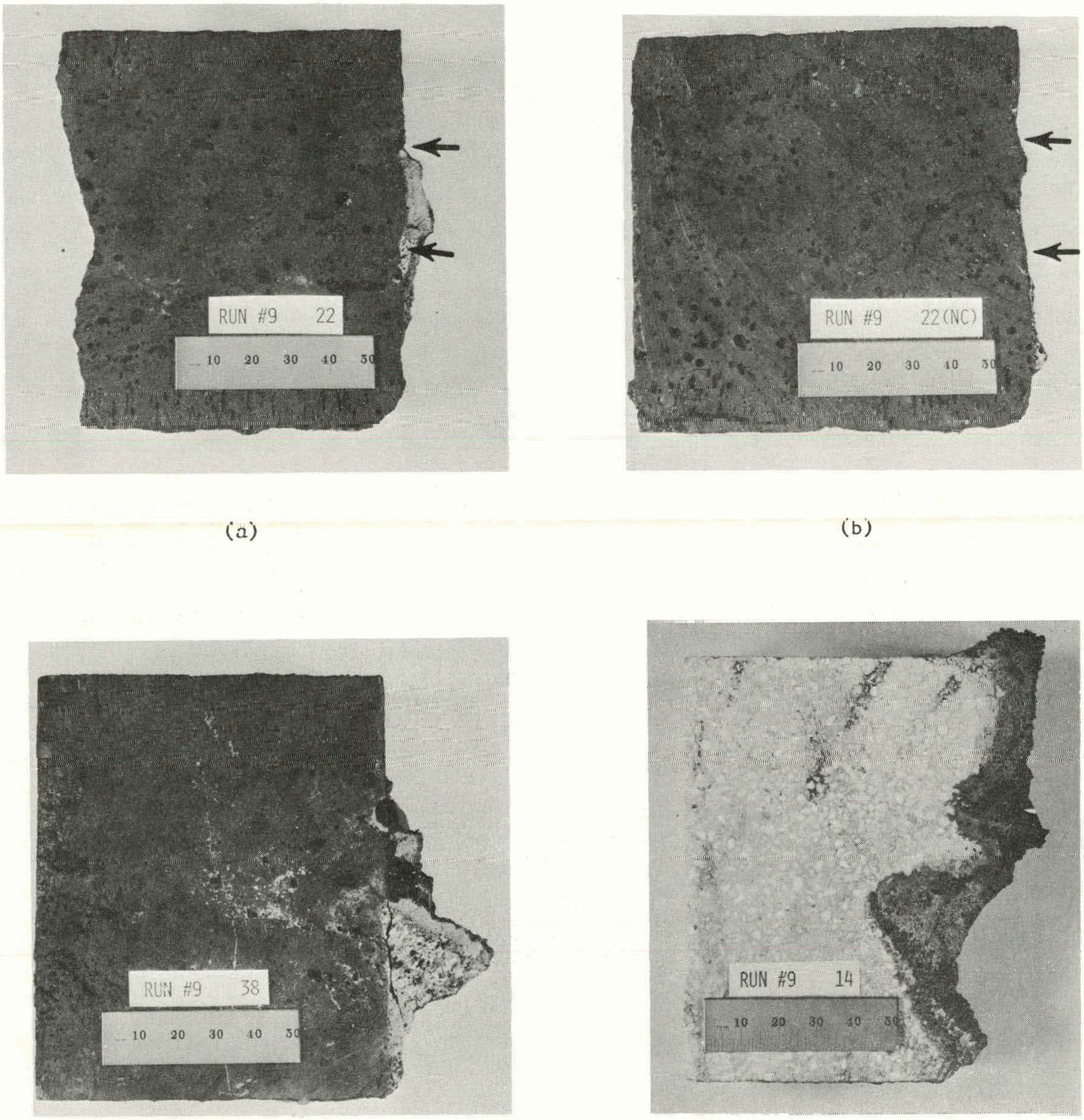

(a) (b)

(c) (d)

Fig. 3. Cut Sections of Refractories Exposed to Slag Attack in Test Run 9. (a) Full-size chrome-spinel (number 22), (b) half-size chrome-spinel (number 22) without water cooling, (c) full-size chrome-alumina (number 38), (d) full-size alumina-silica (number 14), (e) full-size nitride-bonded silicon carbide (number 91), (f) full-size silicate-bonded silicon carbide (number 93), and (g) half-size oxynitride-bonded silicon carbide (number 37). The right-hand vertical faces of (a-d) and the left-hand vertical face of (e) and (f) were exposed to two levels of slag attack. ANL Neg. Nos. 306-78-921, 922.

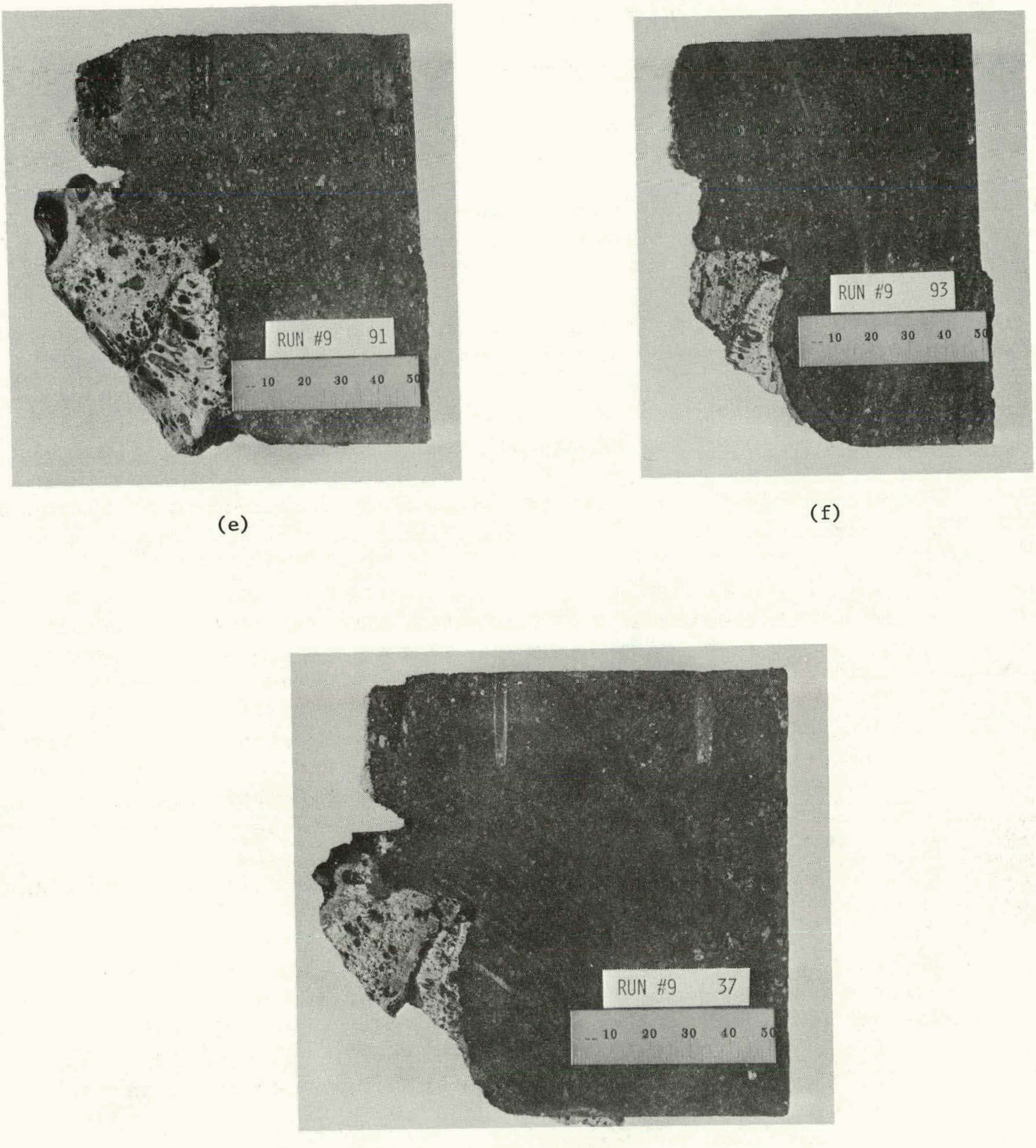

(e)

(f)

(g)

Fig. 3. (Contd.)

Task C -- Application and Development of Nondestructive Evaluation Methods for Coal-conversion Processes *(W.A. Ellingson, K.J. Reimann, W.J. Shack, and C.A. Youngdahl)*

1. Erosive-wear Detection and Monitoring

a. Metallic Transfer Lines

(1) Ultrasonic Studies - Pilot Plants. Field testing of automatic-scanning erosive-wear surveillance instrumentation for metallic transfer lines and fittings of coal-conversion systems was continued this quarter, using the ultrasonic equipment previously installed by ANL at the Bi-Gas Pilot Plant.[1] The instrumentation operated unattended for a 15-day period which encompassed an experimental ∿ 8-h pilot-plant run conducted by Bi-Gas personnel. Twelve waveguide sites that were compatible with scanning at a fixed gain setting (120 dB) were monitored. Each of the four arrays of waveguides at the plant was represented in the set surveyed. The capability for automatic, accurate wall-thickness data retrieval from the plant operating environment was demonstrated. In separate tests with recently improved measurement techniques, satisfactory agreement was demonstrated between values of wall thickness derived from measurements through acoustic waveguides and values obtained by direct-contact ultrasonic techniques.

The following problems, all of which can be overcome, were noted during this test: (1) A 1% drift in recorder calibration with respect to that of the time-analog gate of the pulser-receiver over the 15-day interval between plant visits (this error was eliminated during data reduction); (2) shifts of $\lambda/2$ in the measured Sh-BW distances (see Table IV), probably associated with signal-amplitude variations (ideally, triggering on half-waves with amplitudes near the threshold setting should be avoided); and (3) electrical interference in the temperature trace for the stainless steel array. (In addition, the time-analog gate was subject to zero drift, which would have affected the recorded values if the temperature of the instrument console had not remained relatively constant during the test.)

The capability for consistent data retrieval is illustrated in Table IV. Errors of less than ± 0.13 mm (± 5 mils) are desired, and this precision was achieved for the carbon steel samples when $\lambda/2$ shifts were absent. The effect of the $\lambda/2$ shift [theoretically, 0.58 mm (23 mils)] is also shown in Table IV. For these sites the presence of initial $\lambda/2$ offsets and nonoptimized gain settings should be considered in comparing the results with those reported previously.[2] It is the consistency of the temperature-corrected values and their independence from interference generated by the plant that are of present interest. For the stainless steel waveguide array on the outlet of the gasifier, the measured values differed by as much as 1.3 mm (50 mils) from the expected values, except during one period of constant temperature when errors were typically 0 to 0.25 mm (0 to 10 mils). Improved temperature data from this site may improve the agreement between measured and predicted values. That no measurable wear occurred during the plant run was demonstrated independently of the foregoing, by manually adjusted ultrasonic measurements made pretest and posttest with the plant at ambient temperature.

For Table IV the compensation for changes in acoustic velocity with temperature for A-106B carbon steel was calculated theoretically[3] from the moduli data of Date[4], and densities were calculated from a value of 1.5 x 10^{-5}/°C for the coefficient of linear thermal expansion. For Type 304 stainless steel, the same data source and procedure were used, except that the densities and expansivity data were from Ref. 5. Since the calculated velocities at room temperature differ slightly from handbook values, the ratio of the calculated velocities was used. The thickness indicated at the elevated temperature is expected to be the thermally expanded thickness times the ratio of the acoustic velocity at room temperature (the calibration temperature) to that at the elevated temperature.

The immunity of high-frequency ultrasonic thickness measurements to structure-borne acoustic interference was dramatically demonstrated at the Bi-Gas plant recently. The measurement for waveguide #2, located on the instrumented stainless steel blocked tee and less than 300 mm ($\sim$ 1 ft) from the clean-out port of the tee, was monitored remotely as plant personnel replaced the port cover and tightened the nuts of the sealing clamp with a pneumatic impact-wrench. The 7.5-MHz measurement of distance at a resolution of 0.03 mm was unchanged during the process.

An illustration of measurement accuracy is given in Table V. Values obtained from the waveguides of an accessible tee at the Bi-Gas plant were compared with direct wall-contact measurements taken adjacent to the waveguide sites. The agreement was generally satisfactory; an error of $\sim$ 0.17 mm (6-7 mils) may have been caused in part by error in the assumed shoulder-to-outer-wall distance of 6.35 mm (250 mils). Half-wavelength ($\lambda/2$) offset errors were painstakingly avoided during calibration and measurement in order to achieve this level of accuracy. The offsets were eliminated from the waveguide data as described in Ref. 2, where the resulting values were previously published. The more recent wall-contact data were taken with a 3.5-MHz Aerotech alpha transducer, which does not produce offset errors in ordinary use. The plant was not operated in the interval between the two sets of measurements.

Note: $\lambda/2$ offset errors were discussed in Ref. 2. A clarification of one point appears to be in order. Although it may seem that a full-wave increment is produced by each half-wave rectified alternation in the pulser-receiver, the double time-scale of the pulse-echo technique produces an indicated distance, for each alternation, of an acoustic $\lambda/2$ in the sample material. Thus, offset corrections in increments of $\lambda/2$ are appropriate.

A paper[6] describing the development of automatic instrumentation for remote measurement of erosive wear was completed during the present quarter and contributed to the IEEE 1978 Ultrasonics Symposium in Cherry Hill, New Jersey.

TABLE IV. Examples of Sh-BW Distances[a] Measured at Elevated Temperatures by the Erosive-wear Scanning System, Compared with Predicted Values

				Sh-BW Distance					
				Waveguide #11[d]			Waveguide #19[e]		
	Date and Time	Temp.,[b] °C	k_{cs}[c]	Predicted, in.	Measured, in.	Error, mils	Predicted, in.	Measured, in.	Error, mils
	7/23/78								
	9:00	ambient	1.0000	-	1.021	-	-	1.045	(-1)
	7/28/78								
line pre-heated; plant not in operation	6:00	279	1.0240	1.046	1.047	-1	1.071	1.075	-4
	8:06	283	1.0250	1.047	1.047	0	1.072	1.074	-2
	10:08	292	1.0262	1.048	1.048	0	1.073	1.075	-2
	12:09	294	1.0265	1.048	1.049	-1	1.074	1.075	-1
	14:09	290	1.0260	1.048	1.048	0	1.073	1.075	-2
line at operating temp.; plant in operation	16:09	282	1.0246	1.046	1.048	-2	1.072	1.074	-2
	18:09	281	1.0244	1.046	1.047	-1	1.072	1.072	0
	20:00	277	1.0237	1.045	1.046	-1	1.071	1.074	-3
	22:00	277	1.0237	1.045	1.047	-2	1.071	1.073	-2
	24:00	279	1.0240	1.046	1.048	-2	1.071	1.074	-3
	7/29/78								
	0:10	278	1.0239	1.045	1.025	20[f]	1.071	1.047	24[f]
	0:20	277	1.0237	1.045	1.025	20	1.071	1.047	24
	0:30	328	1.0327	1.054	1.025	29	1.080	1.047	33
cool-down; plant not in operation	0:40	167	1.0105	1.032	1.025	7	1.057	1.047	10
	1:00	197	1.0136	1.035	1.025	10	1.060	1.047	13
	1:30	66	1.0027	1.024	1.025	-1	1.049	1.047	2
	8/7/78								
	9:00	ambient	1.0000	-	1.021	-	-	1.046	-

Legend for Table IV on following page (15).

TABLE IV. Examples of Sh-BW Distances[a] Measured at Elevated Temperatures by the Erosive-wear Scanning System, Compared with Predicted Values

LEGEND

[a] Distance from waveguide shoulder to back wall (inner surface) of feed-line wall without correction for possible $\lambda/2$ offset (1 in. = 1000 mils = 25.4 mm). The effect of a 1% drift in recorder calibration during the period was eliminated from the measured values.

[b] Coal feed-line temperature as reported by Phillips Petroleum personnel at the Bi-Gas pilot plant.

[c] Factor to compensate for acoustic-velocity change and thermal expansion of A-106B steel at elevated temperature, calculated as described in text; the distance measured at room temperature, multiplied by this factor, yields the measurement expected at the stated temperature.

[d] Located on the main coal feed line at a bend near the 6th floor of the plant. Both waveguide and line are of A-106B steel.

[e] Located on the same line at a bend near the 10th floor of the plant.

[f] Attributed to $\lambda/2$ shift error (see text): the $\lambda/2$ value at 5 MHz for carbon steel is 23 mils.

TABLE V. Comparison of Wall Thicknesses, Measured Ultrasonically by Means of Waveguides, with Direct-contact Thickness Measurements at A-106B Carbon Steel Tee in Bi-Gas Main Coal Feed Line

Waveguide Number	Sh-BW Distance[a], in.	Wall Thickness, Tw, Calculated from Sh-BW Distance[b], in.	Wall Thickness, Tc, from Direct-contact Measurements[c], in.	Tw - Tc, mils
26	1.612	1.362		
				-1
			1.363	
				-3
27	1.610	1.360		
				-3
			1.363	
				-3
28	1.610	1.360		
				-4
			1.364	
				+2
29	1.616	1.366		
				+3
			1.363	
				+7
30	1.620	1.370		
				-6
			1.376	
				-1
31	1.625	1.375		

[a] Distance from waveguide shoulder to inner surface of tee (1 in. = 1000 mils = 25.4 mm). Ultrasonic measurements of 3/78.

[b] Nominal distance (i.e., 0.250 in.) from waveguide shoulder to outer surface of tee was subtracted from Sh-BW distance.

[c] ect-contact thickness measurements made 7/22/78 at sites midway between waveguides.

(2) Ultrasonic Studies - Scattering of Acoustic Waves from Rough Surfaces. During the present quarter a computer program was written for analysis of scattering data from the test setup described in the previous report.[1] This program calculates and graphically displays the averaged RF waveform and its power spectrum. A special subprogram has the capability to calculate and graphically display the ratio between the power spectra from a rough and a smooth surface. The resulting data contain only information pertaining to the surface roughness; effects caused by material or transducer variation are eliminated.

The program was first tested by feeding waveforms with known power spectra into the computer (Fig. 4). Subsequently a scan was made over one roughened area of a test block in increments of 1.25 mm (0.05 in). The left side of Fig. 5 shows the RF waveform of the ultrasonic echo from the front surface, and the right side displays the corresponding power spectra. In Fig. 6 the average of the RF waveform and the corresponding power spectrum are displayed.

Two features become immediately apparent. When the transducer progresses from a smooth to a rough portion of the surface a rather large amount of energy is lost by scattering, and the resulting power spectra are low in amplitude. Gain adjustments will have to be implemented if division of power spectra is contemplated. The RF waveform also indicates reflection from the surface and the bottom edge of the grooves. The corresponding power spectra show interference patterns and the periodicity of this interference is most noticeable in the spectrum of the averaged waveforms. During the next quarter, data from different roughened test blocks will be gathered and evaluated.

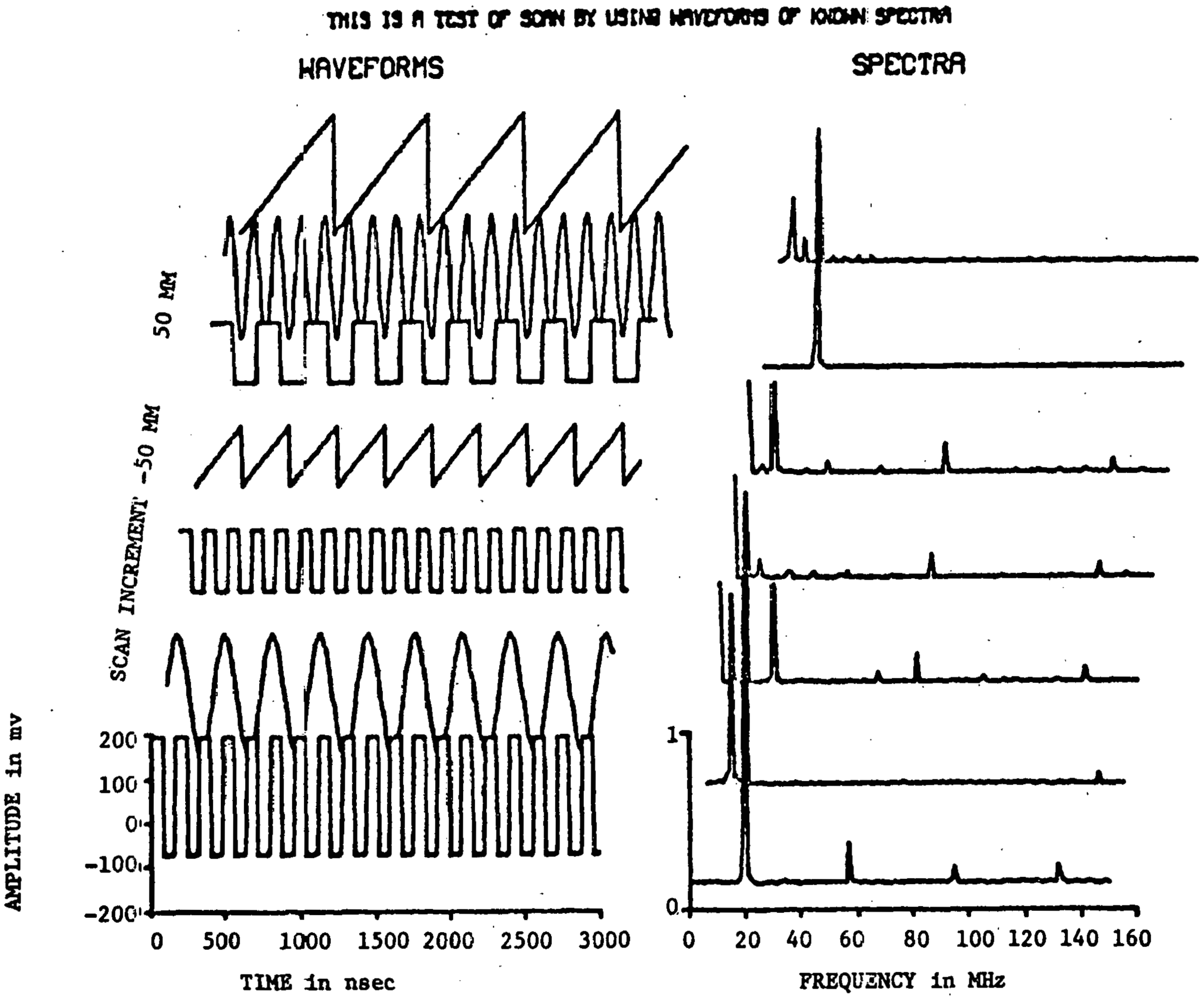

Fig. 4. Waveforms and Associated Power Spectra of Test Signals. Neg. No. MSD-65940.

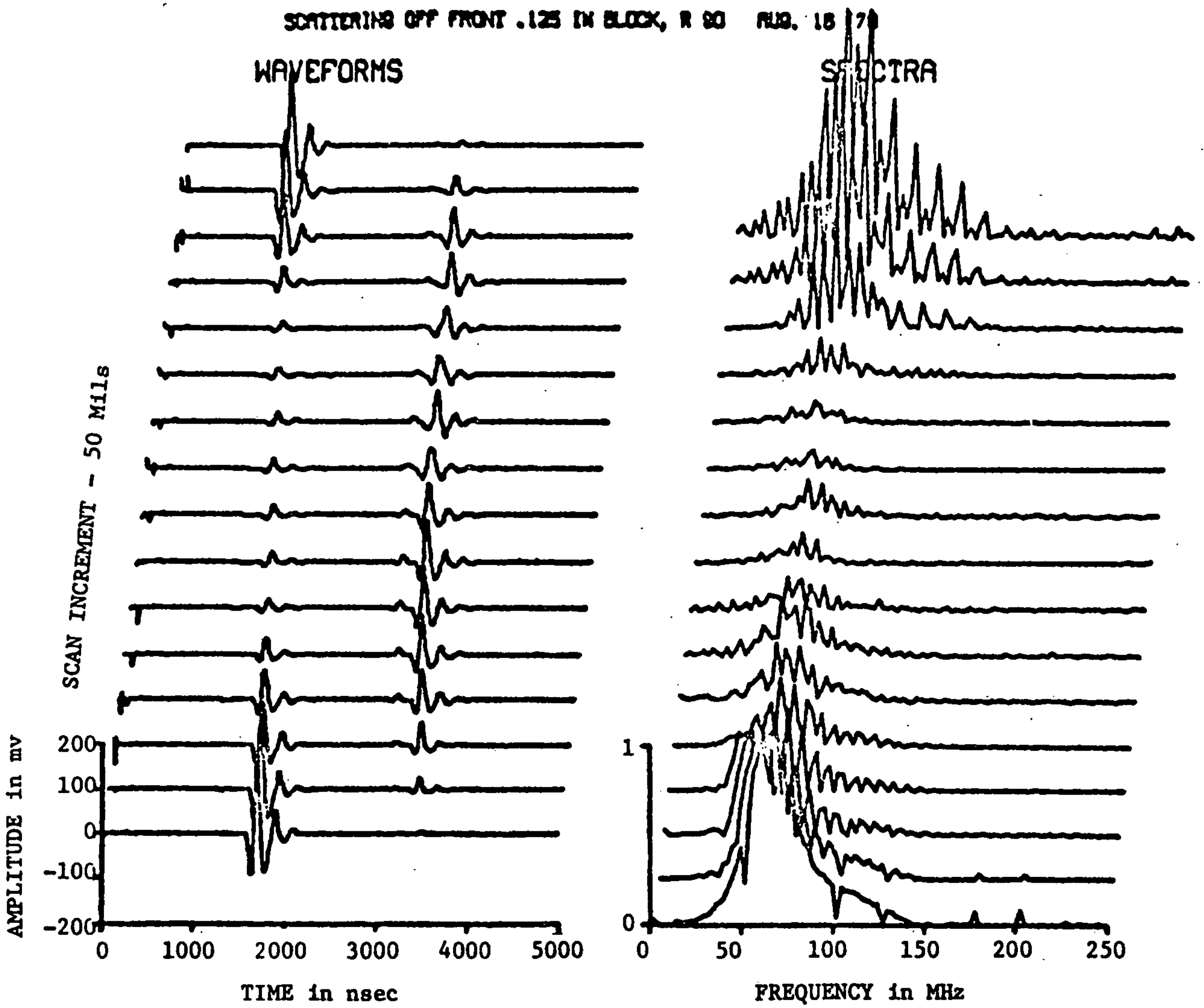

Fig. 5. Ultrasonic Reflection Signals and Associated Power Spectra from a Rough-surface Scan. Neg. No. MSD-65939.

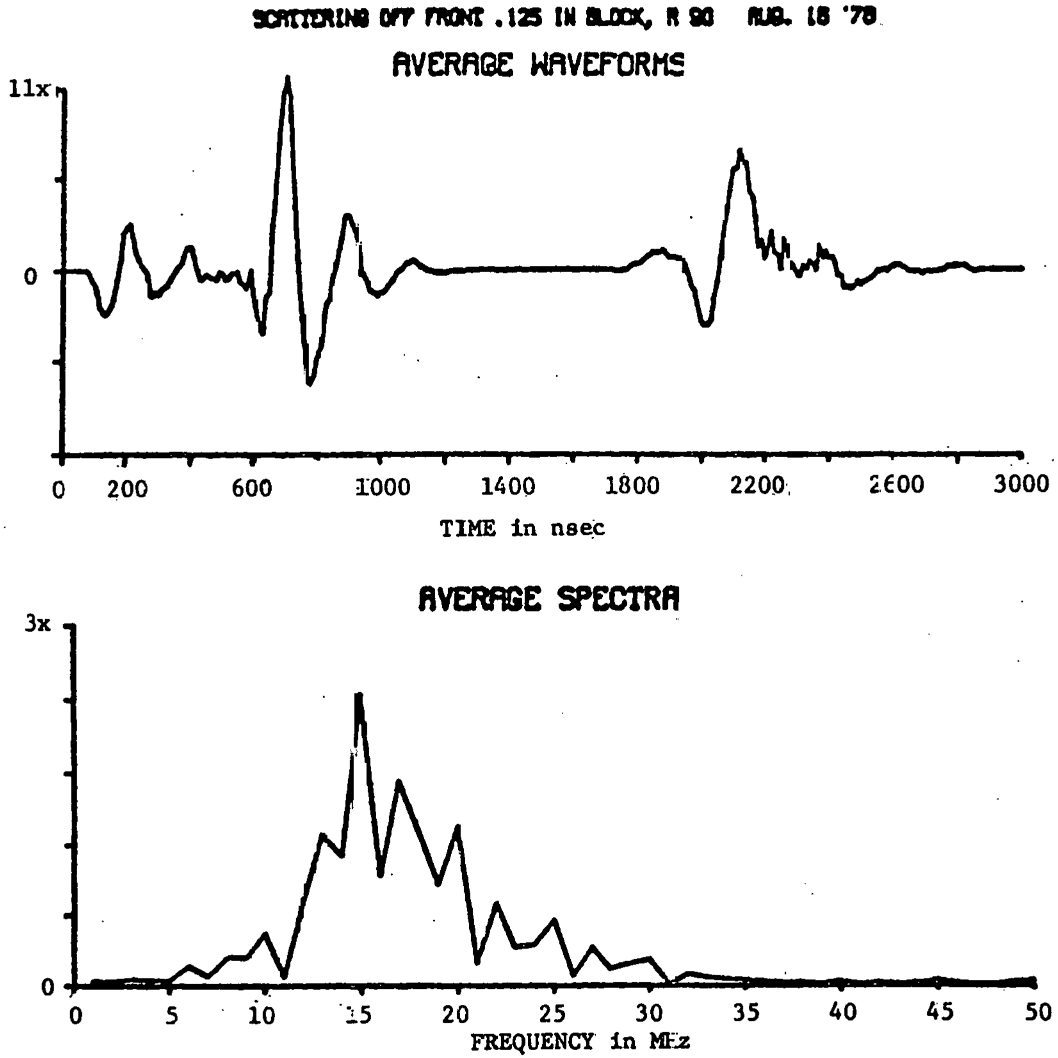

Fig. 6. Averaged RF Waveform and Associated Power Spectrum. Neg. No. MSD-65941.

2. Refractory Installation Practices

a. Detection of Thermally Induced Acoustics from Refractory Concrete Materials

Work has continued this quarter on evaluation of acoustic emission as a means to control the firing schedule of thick, castable-refractory concrete linings of the type envisioned for use in the main process vessels in coal-conversion (gasification, liquefaction) and fluidized-bed (atmospheric and pressurized) plants.

During the present quarter a high-density Castolast-G panel (25 x 30 x 15 cm) was rapidly heated and cooled by means of a glowbar furnace and air quench, respectively. Two "Y"-type hangers were mounted as noted in Fig. 7. Seven type K thermocouples were mounted on the top hanger and three on the bottom hanger (Fig. 8).

Acoustic-emission data were obtained using 2.5-cm-OD x 23-cm-long quartz waveguides, as discussed previously.[1,2,7] A 175-KHz resonant transducer and a broadband transducer were again used throughout the test. An automatic data-acquisition system was employed during this test in an attempt to obtain real-time characteristic slope data. This system is shown schematically in Fig. 9. The output of the amplitude-distribution analyzer was fed to the minicomputer, which was programmed for real-time characteristic slope determination.

The hot-face temperature versus time data are shown in Fig. 10. The maximum heating rate was about 225°C/hr. The remainder of the data will be presented next quarter.

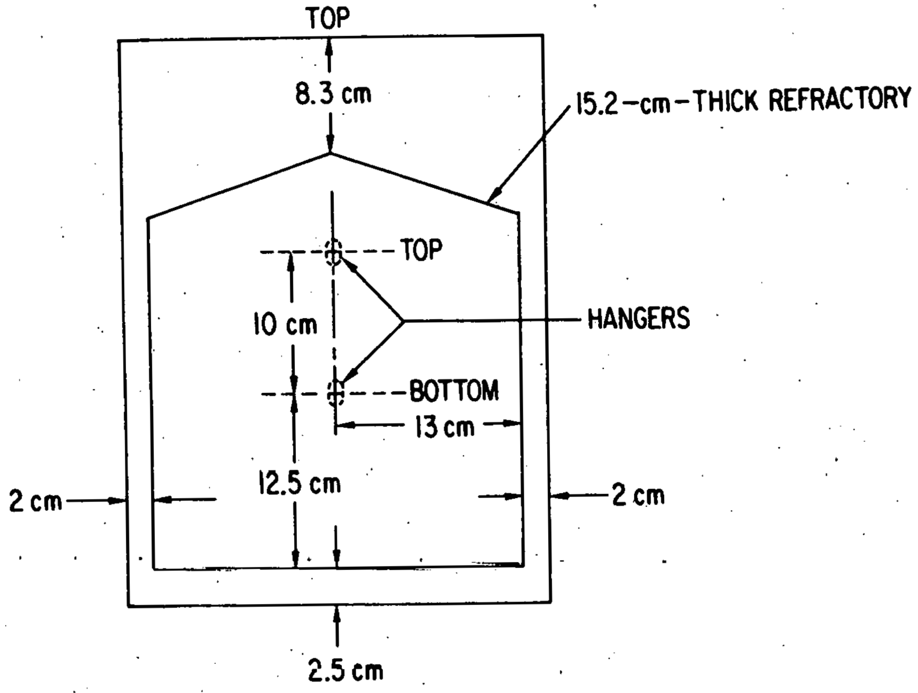

Fig. 7. Front View of Refractory Panel Showing Hanger Locations and Overall Dimensions. Neg. No. MSD-65885.

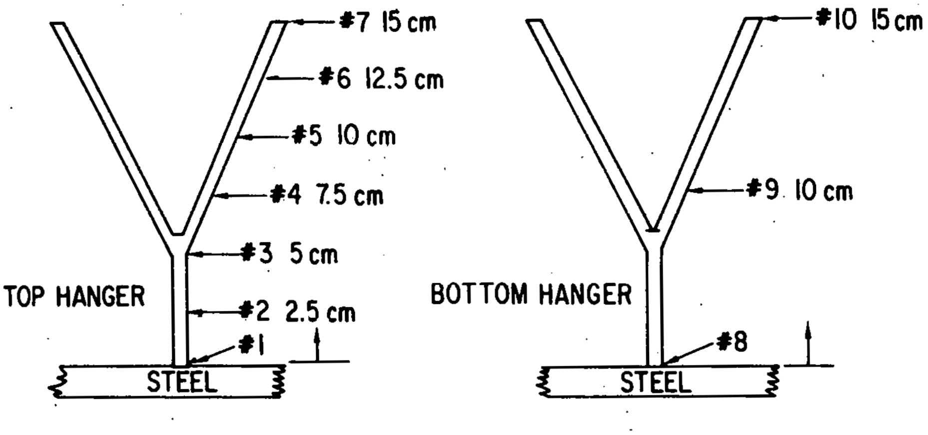

Fig. 8. Schematic Diagram Showing Thermocouple Locations on Hangers. Neg. No. MSD-65888.

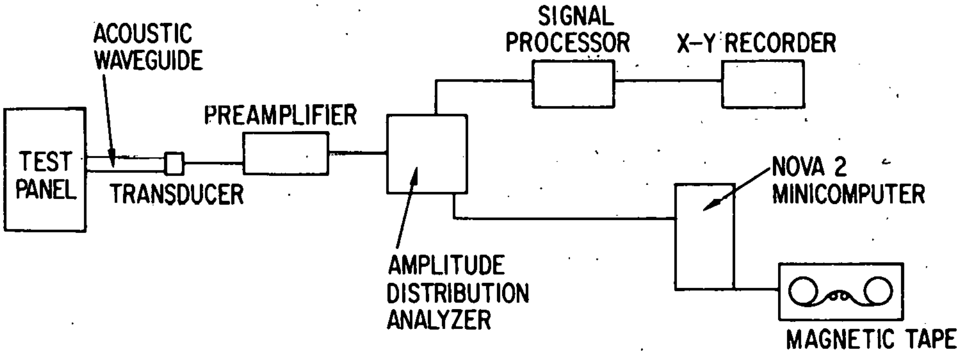

Fig. 9. Schematic Diagram of Automatic Data-acquisition System. Neg. No. MSD-65887.

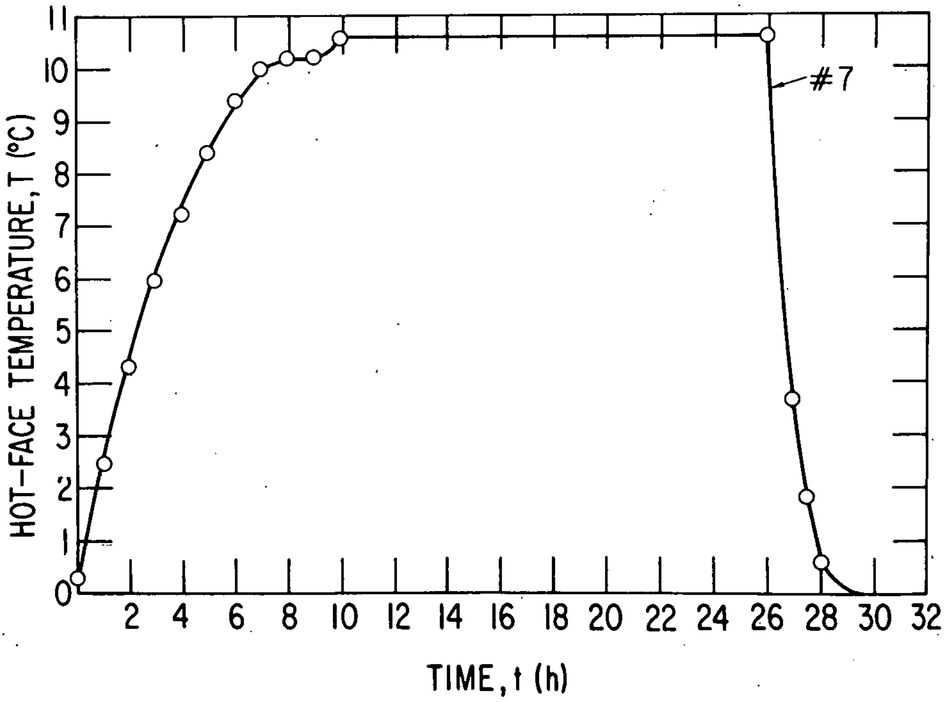

Fig. 10. Hot-face Temperature of Panel as Function of Time. Neg. No. MSD-65886.

3. Component Inspection

a. Acoustic Monitoring of Valves

The two acoustic instruments for valve-leak testing, described in the previous quarterly report[1], were received by ANL during this quarter. Because the unit provided by the Naval Ship Research and Development Laboratory had been designed for intermittent use and a continuous capability was needed, an auxiliary power supply was constructed and installed in the unit. After preliminary tests at ANL, the instruments were taken to the Morgantown Energy Technology Center (West Virginia) during August and given initial tests on a high-pressure, 6-in. ball valve in the valve-leak test facility there. Additional tests of the performance of the acoustic detectors are to be conducted at Morgantown, and results will be presented in the next quarterly report.

Task D -- Corrosion Behavior of Materials

1. Corrosion in Gasification Environments

(K. Natesan)

The objectives of this program are to (1) develop uniaxial tensile data on four commercial alloys upon exposure to multicomponent gas environments, (2) experimentally evaluate the high-temperature corrosion behavior of iron- and nickel-base alloys in gas environments with a wide range of oxygen, sulfur, and carbon potentials, and (3) develop a systems approach based upon available thermodynamic and kinetic information so that possible corrosion problems in different coal-conversion processes can be evaluated.

The experimental program used to generate uniaxial tensile data on four iron- and nickel-base alloys upon exposure to multicomponent gas environments was discussed in detail in an earlier report.[8] A description of the experimental system and the chemical composition of the alloys and gas mixtures used in the program were given in another report.[2] The calculated values for the oxygen and sulfur partial pressures established by the gas mixtures in different runs were given in the previous quarterly report.[1]

During the present quarter, 3.6-Ms (1000-h) exposures of corrosion specimens and uniaxial tensile specimens to gas mixture 1B at 871°C and 1A and 2A at 982°C were completed. The corrosion specimens from different experimental runs were analyzed using scanning-electron microscopy (SEM) and the energy-dispersive x-ray (EDAX) analyzer. The type and thickness of corrosion-product scale and the depth of intergranular penetration in different specimens were evaluated. The results are listed in Tables VI-VIII for exposure temperatures of 750, 871, and 982°C, respectively. Postexposure tensile tests of the specimens were conducted in vacuum at an initial strain rate of $4.1 \times 10^{-4}\ s^{-1}$. The load-elongation data from the tensile tests were converted to true stress-true strain curves for the alloys in the as-received condition and after exposure to the multicomponent gas environments. In general, the flow stress of the material decreases after exposure to complex gas mixtures when compared with that of the material in the as-received condition. The engineering tensile properties, such as 0.2% yield stress, ultimate tensile strength (UTS), uniform strain, and total elongation were also evaluated from the load-elongation data. Tables IX through XI show listings of these properties for the alloys in the as-received condition and after 3.6-Ms (1000-h) exposures to complex gas mixtures at test temperatures of 750, 871, and 982°C, respectively. The results show that preexposure of the materials to multicomponent gas mixtures leads to a decrease in 0.2% yield stress and UTS with only minimal changes in the uniform strain over the range of $\sim$4 to 13%. The results at 750°C also show that the materials exposed to the "IB" mixture exhibited a much larger degradation in the strength properties than those exposed to "A"-series mixtures. This difference in behavior can be attributed to the lower oxygen partial pressure established by the 1B mixture, as indicated in Table VI.

After the mechanical tests were completed, the cross sections and fracture surfaces of the tensile specimens were examined by SEM and the x-ray analyzer. Figures 11-14 show SEM photographs of the cross sections of Incoloy 800, Type 310 stainless steel, Inconel 671, and U. S. Steel Alloy 18-18-2, respectively, after a 3.6-Ms exposure to a complex gas mixture at 982°C (run A01A982). Also shown in these figures are the metallic-element (chromium, iron, nickel, silicon, and titanium) and sulfur distributions in the scale/alloy interface regions of the samples. The photographs show that the scales developed on Incoloy 800 and Type 310 stainless steel in run A01A982 are a mixture of Cr-rich oxide and Cr sulfide. Inconel 671 alloy developed a Cr-rich oxide scale with a small amount of sulfur in the scale region. U. S. Steel Alloy 18-18-2 developed a Cr-oxide/Si-oxide duplex scale which seems to inhibit penetration of sulfur into the alloy. The specimens from other experiments are presently being examined.

Additional experiments are being conducted to evaluate the effect of variations in the exposure environment on the uniaxial tensile behavior of the selected alloys.

TABLE VI. Corrosion-product Analysis of Specimens After 3.6-Ms Exposure to Complex Gas Mixtures at 750°C

Run No.	p_{O_2}, atm	p_{S_2}, atm	a_c	Alloy	Scale Thickness, µm	Depth of Penetration, µm	Type of Scale
A01A750	1.7×10^{-20}	3.8×10^{-8}	0.056	Incoloy 800	6.0	16.0	Cr-rich oxide
				Type 310 SS	6.3	5.0	Cr-rich oxide
				Inconel 671	3.1	13.8	Cr oxide
				U.S. Steel Alloy 18-18-2	63.8	31.9	Cr/Fe sulfide
E12A750	5.9×10^{-21}	2.7×10^{-8}	0.125	Incoloy 800	15.0	30.8	Cr-rich oxide
				Type 310 SS	4.7	23.5	Cr oxide/sulfide
				Inconel 671	3.5	18.8	Cr oxide
				U.S. Steel Alloy 18-18-2	7.1	20.5	Cr oxide/sulfide
B03A750	2.2×10^{-21}	2.9×10^{-8}	0.325	Incoloy 800	10.0	26.7	Cr-rich oxide
				Type 310 SS	5.7	20.0	Cr-rich oxide
				Inconel 671	29.5	18.9	Cr sulfide/(Cr,Ni) sulfide
				U.S. Steel Alloy 18-18-2	43.1	30.8	Fe/(Fe,Ni) sulfide
C01B750	6.7×10^{-22}	9.9×10^{-9}	0.487	Incoloy 800	235.3	258.9	(Cr,Fe) sulfide
				Type 310 SS	196.9	141.5	(Cr,Ni) sulfide
				Inconel 671	20.0	42.5	Cr sulfide
				U.S. Steel Alloy 18-18-2	160.0	91.4	Fe sulfide

TABLE VII. Corrosion-product Analysis of Specimens after 3.6-Ms Exposure to Complex Gas Mixtures at 871°C

Run No.	p_{O_2}, atm	p_{S_2}, atm	a_c	Alloy	Scale Thickness, µm	Depth of Penetration, µm	Type of Scale
A01A871	1.1×10^{-17}	4.0×10^{-7}	0.010	Incoloy 800	-	-	Sulfide
				Type 310 SS	34.0	68.6	(Cr,Mn) oxide
				Inconel 671	22.8	57.1	(Cr,Ni) sulfide
				U.S. Steel Alloy 18-18-2	-	-	Sulfide
E12A871	3.6×10^{-18}	2.7×10^{-7}	0.023	Incoloy 800	694.0	764.0	(Fe,Ni) sulfide
				Type 310 SS			
				Inconel 671	25.6	410.0	Cr sulfide
				U.S. Steel Alloy 18-18-2			
B03A871	1.4×10^{-18}	2.8×10^{-7}	0.056	Incoloy 800	16.7	50	Cr sulfide
				Type 310 SS	-	-	
				Inconel 671	4.5	16	Cr-rich oxide
				U.S. Steel Alloy 18-18-2	-	-	
C01B871	3.2×10^{-19}	8.7×10^{-8}	0.096	Incoloy 800	50	212.5	Fe sulfide
				Type 310 SS	586	759	(Fe,Cr) sulfide
				Inconel 671	-	-	
				U.S. Steel Alloy 18-18-2	-	-	Cr sulfide

TABLE VIII. Corrosion-product Analysis of specimens After 3.6-Ms Exposure to Complex Gas Mixtures at 982°C

Run No.	p_{O_2}, atm	p_{S_2}, atm	a_c	Alloy	Scale Thickness, µm	Depth of Penetration, µm	Type of Scale
A01A982	1.3×10^{-15}	2.4×10^{-6}	0.003	Incoloy 800	20.0	114.3	Cr oxide/sulfide
				Type 310 SS	18.5	98.5	Cr oxide/sulfide
				Inconel 671	6.2	100.2	Cr oxide
				U.S. Steel Alloy 18-18-2	12.3	73.8	Cr oxide/Si oxide
E12A982	4.5×10^{-16}	1.5×10^{-6}	0.006	Incoloy 800	416.7	335.1	Cr/(Cr,Fe) sulfide
				Type 310 SS	301.9	532.7	Cr sulfide
				Inconel 671	7.1	113.6	Cr oxide
				U.S. Steel Alloy 18-18-2	710.2	580.6	Cr oxide, Fe sulfide

TABLE IX. Uniaxial Tensile Properties of Four Alloys in the As-received Condition and After 3.6-Ms Exposures to Multicomponent Gas Environments at 750°C

Alloy	Treatment	0.2% Yield Stress, MPa	Ultimate Tensile Strength, MPa	Uniform Strain, %	Total Elongation, %
Incoloy 800	As-received	91.0	226.7	4	136
	A01A750	53.3	204.2	10.8	100.4
	E12A750	40.5	200.0	8.8	70.4
	B03A750	69.9	190.3	13.3	90.0
	C01B750	64.6	138.2	8.6	55.4
Type 310 Stainless Steel	As-received	49.2	257.9	4	38
	A01A750	43.2	219.4	8.1	36.4
	E12A750	36.1	222.9	9.4	27.5
	B03A750	-	216.0	7.4	38.9
	C01B750	-	188.9	7.9	29.0
U.S. Steel Alloy 18-18-2	As-received	63.5	191.2	8	70
	A01A750	57.6	181.9	12.3	64.5
	E12A750	43.7	182.6	9.8	62.5
	B03A750	-	163.9	6.9	43.8
	C01B750	-	171.5	8.4	58.1
Inconel 671	As-received	49.2	339.0	9	32
	A01A750	48.5	265.3	3.9	77
	E12A750	45.1	256.9	5.9	54.1
	B03A750	-	223.6	3.9	107.3
	C01B750	-	241.7	4.3	98.4

TABLE X. Uniaxial Tensile Properties of Four Alloys in the As-received Condition and After 3.6-Ms Exposures to Multicomponent Gas Environments at 871°C

Alloy	Treatment	0.2% Yield Stress, MPa	Ultimate Tensile Strength, MPa	Uniform Strain, %	Total Elongation, %
Incoloy 800	As-received	30.7	119.7	4	123
	A01A871	-	51.4	2.4	8.4
	E12A871	41.3	75.7	2.5	46.4
	B03A871	60.2	100.0	7.9	149.6
	C01B871	-	88.2	4.9	77.5
Type 310 Stainless Steel	As-received	43.0	138.5	3	48
	A01A871	20.0	106.5	8.9	76
	E12A871	-	Sample Embrittled	-	-
	B03A871	-	Sample Embrittled	-	-
	C01B871	-	97.9	5.9	66.9
U.S. Steel Alloy 18-18-2	As-received	36.8	94.5	3	71
	A01A871		Sample Corroded		
	E12A871		Sample Embrittled		
	B03A871		Sample Embrittled		
	C01B871		Sample Corroded		
Inconel 671	As-received	42.0	141.1	5	87
	A01A871	27.3	105.9	4.9	172
	E12A871	43.1	88.9	3.5	74.3
	B03A871	62.2	118.0	3.0	163.0
	C01B871		Sample Corroded		

TABLE XI. Uniaxial Tensile Properties of Four Alloys in the As-received Condition and After 3.6-Ms Exposures to Multicomponent Gas Environments at 982°C

Alloy	Treatment	0.2% Yield Stress, MPa	Ultimate Tensile Strength, MPa	Uniform Strain, %	Total Elongation, %
Incoloy 800	As-received	29.7	59.7	11.1	120.1
	A01A982	27.1	47.9	8.6	52.9
	E12A982		Sampled Embrittled		
Type 310 Stainless Steel	As-received	25.4	55.0	14.7	78.1
	A01A982	25.7	45.8	13.5	75.1
	E12A982		Sampled Embrittled		
U.S. Steel Alloy 18-18-2	As-received	30.4	52.0	2.0	67.9
	A01A982	26.7	41.7	16.0	86.1
	E12A982		Sample Corroded		
Inconel 671	As-received	22.4	50.7	4.3	234.4
	A01A982	24.3	54.4	7.4	68.9
	E12A982	24.7	53.5	7.4	68.9

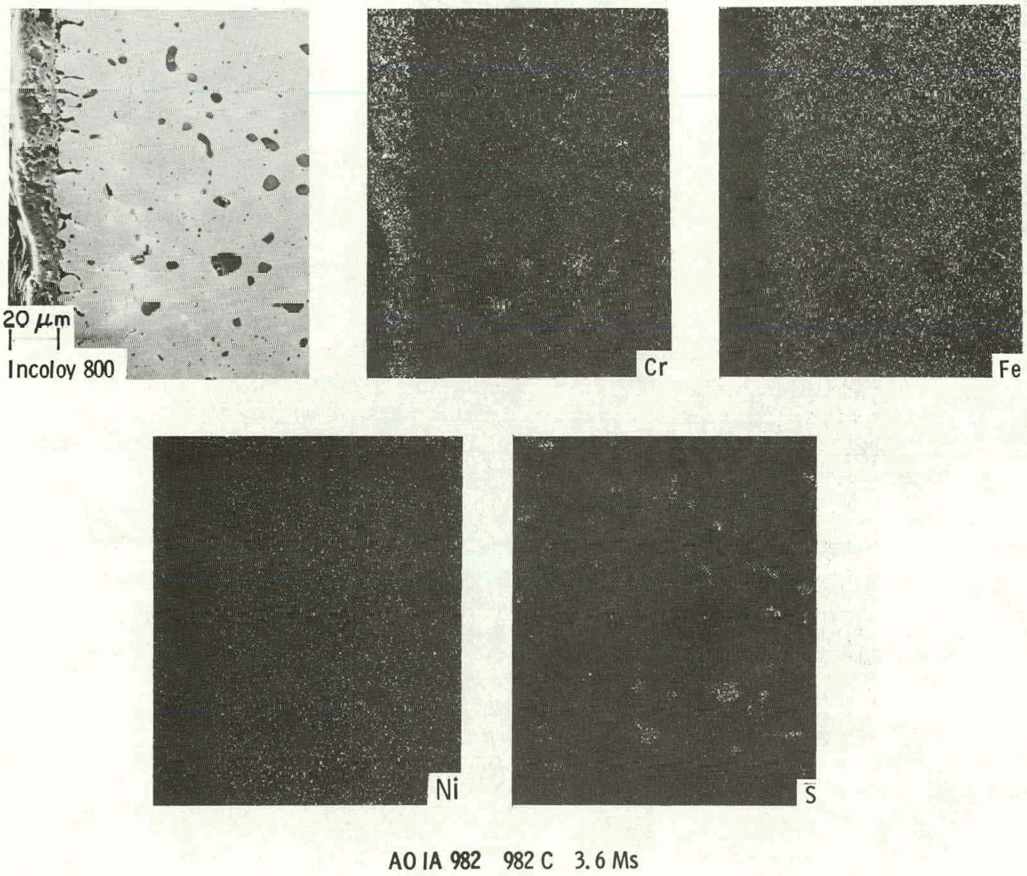

Fig. 11. X-ray Photograph and Cr, Fe, Ni, and S Distribution in Incoloy 800 Specimen After a 3.6-Ms Exposure to a Complex Gas Mixture at 982°C (Run A01A982). In the distribution pictures, light regions indicate high concentrations of the respective elements. ANL Neg. No. 306-78-811A

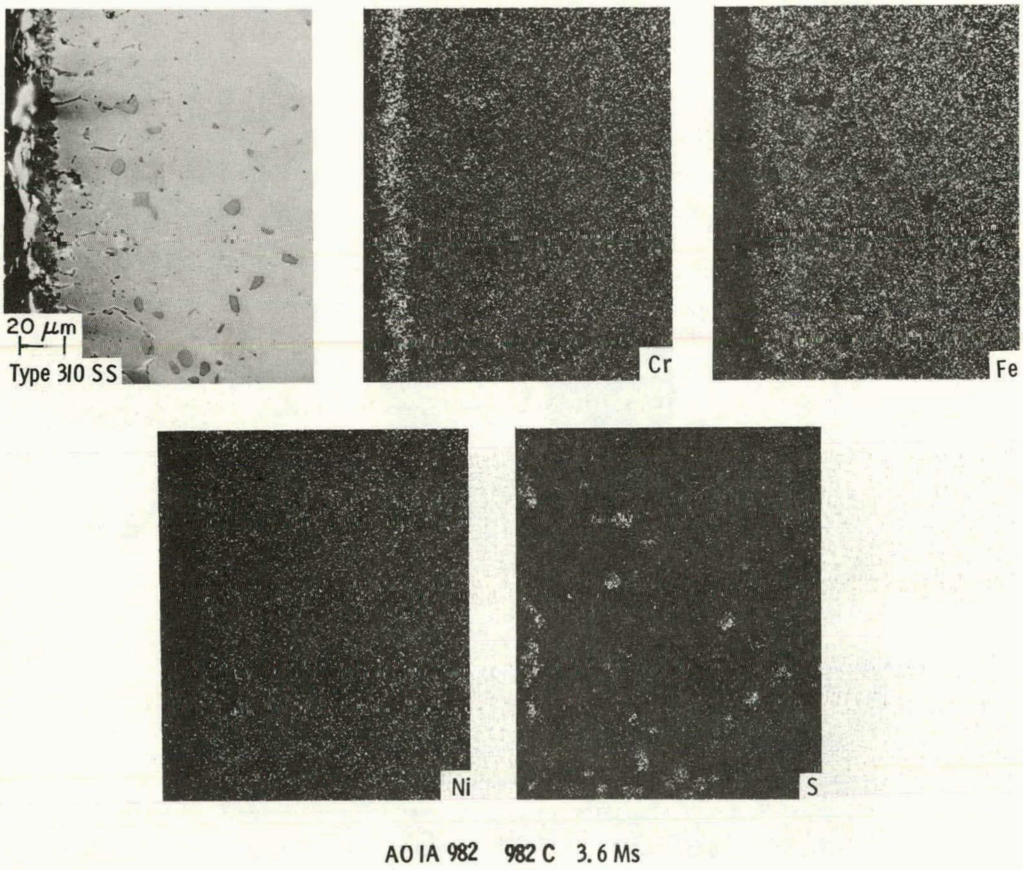

Fig. 12. X-ray Photograph and Cr, Fe, Ni, and S Distribution in Type 310 Stainless Steel Specimen After a 3.6-Ms Exposure to a Complex Gas Mixture at 982°C (Run A01A982.). In the distribution pictures, light regions indicate high concentrations of the respective elements. ANL Neg. No. 306-78-805.

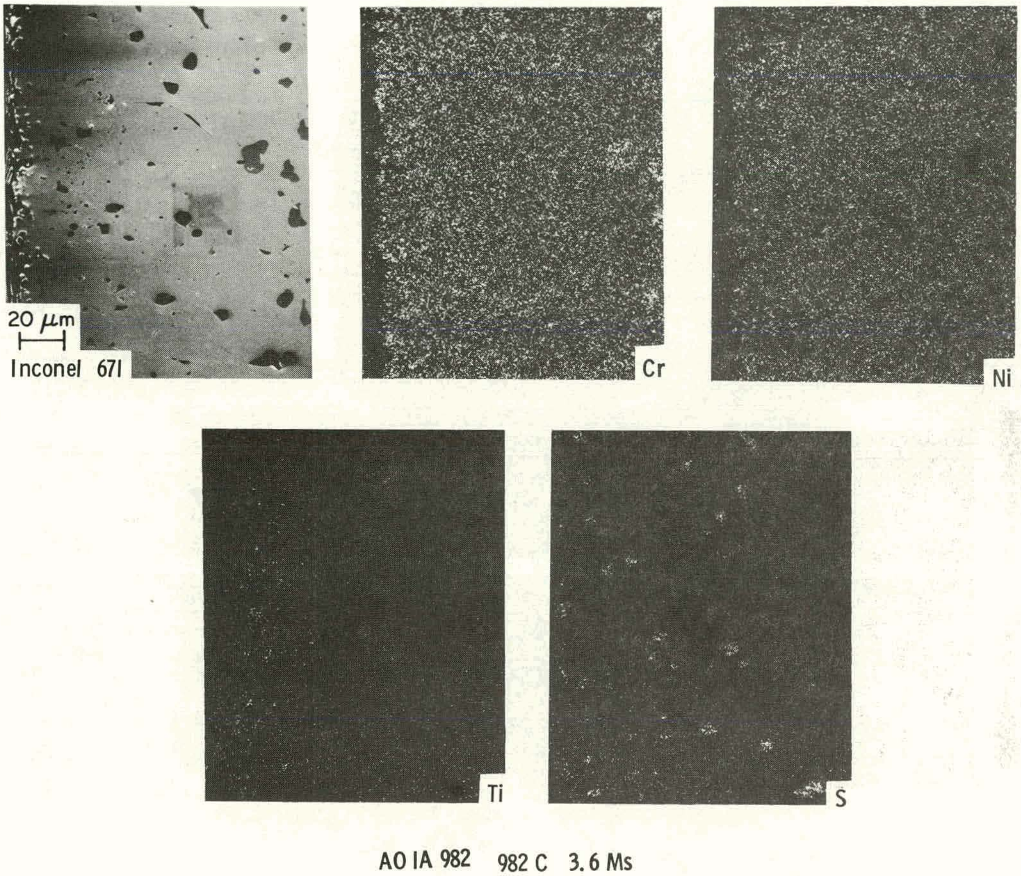

Fig. 13. X-ray Photograph and Cr, Ni, Ti, and S Distribution in Inconel 671 Specimen After a 3.6-Ms Exposure to a Complex Gas Mixture at 982°C (Run A01A982). In the distribution pictures, light regions indicate high concentrations of the respective elements. ANL Neg. No. 306-78-814.

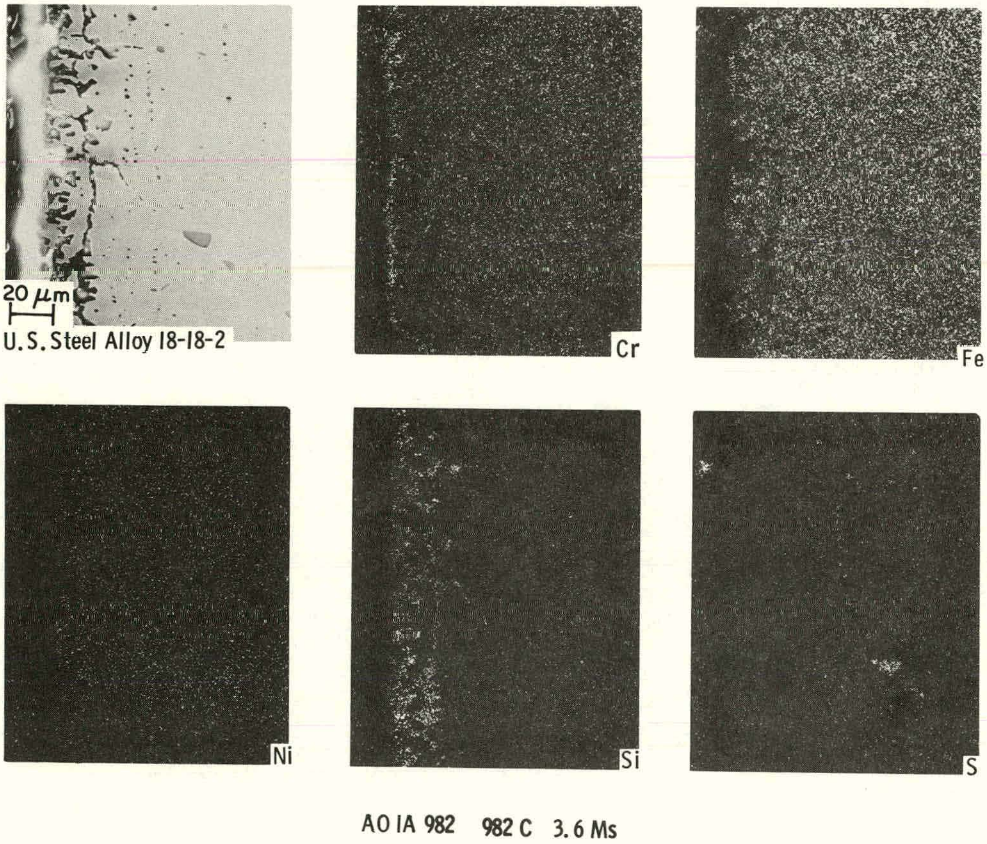

Fig. 14. X-ray Photograph and Cr, Fe, Ni, Si, and S Distribution in U.S. Steel Alloy 18-18-2 Specimen After a 3.6-Ms Exposure to a Complex Gas Mixture at 982°C (Run A01A982). In the distribution pictures, light regions indicate high concentrations of the respective elements. ANL Neg. No. 306-78-800.

2. Corrosion in Atmospheric Fluidized-bed Environments *(O.K. Chopra)*

The effects of NaCl and $CaCl_2$ on the corrosion behavior of materials in a fluidized-bed combustion environment have been evaluated for various salt additions. The results of a metallographic examination of the corrosion coupons exposed in the presence and absence of salt are presented in this report. The composition of the materials is given in Table XII. Corrosion coupons were exposed inside and above a fluidized bed at 1123 K for 100 h. The bed material and the fluidizing gas composition for the various tests are given in Table XIII. In runs 3, 4, and 5, salt was introduced in pretreated dolomite prepared by soaking in salt solution and drying. Small portions of the treated stone were periodically introduced into the fluidized bed. The fluidized-bed vessel was equipped with an overflow tube which maintained a constant bed level. For these runs, the fluidizing gas contained 3200 ppm SO_2. After reacting with limestone, the gas had an SO_2 content of 200-500 ppm.

a. Metallographic Examination

The corrosive attack in all the specimens was primarily oxidation with some sulfidation of the material. In general, the addition of salt to the fluidized bed increased the corrosion rates. The average thickness of the surface scales and the depth of corrosion-product penetration for the specimens exposed inside and above the fluidized bed are shown in Figs. 15 and 16, respectively. In the absence of salt, all materials, with the exception of Inconel 601, developed 2- to 3-μm-thick surface scales when exposed either above or in the fluidized bed that contained sulfated dolomite. The corrosive attack under the surface scale in these specimens was minimal. For the same environmental conditions, Inconel 601 specimens suffered considerable internal attack because the exposure temperature was ∿50 K higher, i.e., ∿1173 K.

As shown in Figs. 15 and 16, the addition of salt to the fluidized bed increased the corrosive attack in all the materials. The iron-base alloys, namely Types 304, 316, and 310 stainless steel, fared better than the high-nickel alloys. For these stainless steels, a variation in the amount of NaCl in the bed had little or no effect on their corrosion behavior. In the presence of NaCl, the average value of the total corrosive attack, i.e., the scale thickness plus the depth of penetration, observed in Types 304, 316, and 310 stainless steel was ∿20 μm as compared to ∿4 μm in the absence of salt and ∿8 μm in the presence of 0.1 mole % $CaCl_2$.

The corrosion behavior of the nickel-base alloys, i.e., Inconel 600, Inconel 601, and RA333, showed a dependence on the amount of salt in the fluidized bed. The addition of solid NaCl (run 2) increased the corrosive attack drastically, i.e., thick surface scales and extensive internal attack occurred. The specimens exposed above the bed generally showed greater corrosive penetration than those exposed inside the bed. However, in the presence of 1.0 mole % NaCl or 0.1 mole % $CaCl_2$, the average total corrosion attack for these alloys was ∿20 μm.

Detailed metallographic examination was made of all the specimens to determine the distribution of corrosion products. Figures 17 to 22 show scanning-electron micrographs of the cross sections of specimens of Types 304 and 310 stainless steel, Incoloy 800, Inconel 600, Inconel 601, and RA333 exposed under different test conditions. The specimens exposed to the environment with NaCl or $CaCl_2$ exhibited large cavities along the grain boundaries. Micrographs of the specimens indicate that in the presence of salt, the internal corrosive attack is primarily caused by the preferential oxidation of the carbide phases. Carbon from the carbides diffuses into the material and reprecipitates ahead of the oxidation front, as shown in Figs. 19 and 22b. These specimens showed a depletion of chromium in the surface region. The x-ray microprobe line analyses for nickel, iron, and chromium on Incoloy 800 specimens, which were exposed above the bed without and with NaCl, are shown in Figs. 23a and 23b, respectively. In the absence of NaCl, the distribution of nickel, iron, and chromium in the specimen is relatively uniform. However, in the presence of NaCl, the surface region is depleted in chromium and iron to a depth of ∿60 μm. The specimen matrix in this region consists primarily of nickel.

Scanning-electron micrographs and EDAX analyses of the surface of the scales formed on Incoloy 800 specimens that were exposed above the bed are shown in Fig. 24. In the absence of NaCl (Fig. 24a), a continuous oxide scale formed on the specimen surface. The major elements in the scale are chromium, manganese, and iron. Minor amounts of calcium, magnesium, silicon, sulfur, aluminum, and titanium are also observed. Sulfur is probably present in calcium sulfate particles that deposit on the scale. When NaCl is present in the bed (Fig. 24b), the specimen surface is quite corroded and the metal grains underneath the scale are exposed. The EDAX analysis of the surface shows the presence of nickel, iron, and silicon.

These results indicate that NaCl causes the destruction of the normally protective oxide scales. This process leads to a continuous depletion of chromium and iron in the specimen matrix. The absence of a stable and adherent oxide scale causes internal oxidation and sulfidation of the alloys. The sulfides are always observed ahead of the oxidation front.

For most of the alloys, the internal corrosive attack consists of three distinct zones. The zone near the surface consists of internal oxidation. The matrix is depleted of chromium and shows iron-silicon oxides along the grain boundaries. The second zone consists of patches of chromium and manganese sulfides. In this region, the partial pressure of oxygen is low and chromium reacts preferentially with sulfur to form sulfides. The internal oxidation and sulfidation zones are free of carbide particles. The carbides in these zones are either oxidized or they dissolve, and the carbon diffuses into the material and reprecipitates as chromium-rich carbides ahead of the sulfidation zone. The third zone consists of these reprecipitated carbide particles.

b. Effect of Temperature

To evaluate the effect of temperature on the corrosion behavior of materials in the presence of salt, corrosion specimens were placed at different heights above the fluidized bed. The temperature of the specimens varied from 1123 to 723 K. For these tests, the fluidized bed contained 3.0 mole % NaCl. Micrographs of Types 304 and 310 stainless steel specimens exposed inside and above the bed at different temperatures are shown in Figs. 25 and 26, respectively.

The corrosion behavior of the specimens that were exposed inside and above the bed at 1123 K was similar to that described in the previous section. However, the specimens exposed above the bed at lower temperatures showed considerable corrosive attack. The total corrosion depth in Types 304 and 310 stainless steel specimens at 923 K is 80 and 50 μm, respectively, and at 823 K the values are 600 and 100 μm, respectively. At these temperatures, the surface scales consist of an outer layer of iron oxide with an inner layer of mixed oxides of iron and chromium. The alloy matrix shows extensive internal sulfidation and oxidation.

The x-ray microprobe line analyses for iron, chromium, nickel, oxygen, and sulfur on Types 304 stainless steel specimens exposed at 923 K above the bed containing NaCl are shown in Fig. 27. The relative concentration of these elements shows that the outer surface scale consists mainly of iron and oxygen. The inner scale contains iron, chromium, and oxygen. The region below the oxides consists of nickel, iron, and sulfur. The x-ray images for the above elements and chlorine are shown in Fig. 28 along with a micrograph of the surface scale on the same specimen. The distribution of the various elements shows the two oxide layers and the region of internal sulfidation and oxidation. The x-ray image for chlorine shows that this element is present in regions which show a higher concentration of sulfur. This behavior was observed in all the specimens exposed at 923 and 823 K. Chlorine was observed in the region between the oxide layer and the area of internal sulfidation. The sulfide/mixed-oxide and the mixed-oxide/iron-oxide interfaces observed in Type 304 stainless steel specimens exposed at 823 K are shown in Figs. 29a and 29b, respectively. Cubes of NaCl can be clearly seen in the sulfide region.

c. Conclusions

1. The addition of NaCl or $CaCl_2$ to the fluidized bed increases the corrosion rates.
2. In the presence of salt, Types 304, 316, and 310 stainless steel perform better than the high-nickel alloys.
3. The corrosion behavior of stainless steels is relatively insensitive to the amount of NaCl in the bed.
4. The total corrosive attack in Inconel 600, Inconel 601, and RA333 in the presence of 1.0 mole % NaCl or 0.1 mole % $CaCl_2$ is comparable to that of the stainless steels.
5. The internal corrosive attack consists of three distinct zones: internal oxidation, internal sulfidation, and a carburized zone where the carbon from the outer zone reprecipitates as chromium-rich carbides.

6. Specimens exposed above the fluidized bed at 923 and 823 K show extensive corrosive attack.

TABLE XII. Composition[a] of Alloys

	Fe	Ni	Cr	Mo	Mn	Si	C	Others
Inconel 600	8.0	Bal.	15.5	-	0.5	0.25	0.08	
Inconel 601	14.1	Bal.	23.0	-	0.5	0.25	0.05	1.35 Al, 0.25 Cu
RA333	18.0	Bal.	25.0	3.0	1.5	1.25	0.05	
Type 304 SS	Bal.	9.5	19.0	-	2.0	0.50	0.08	
Type 316 SS	Bal.	12.0	17.0	2.5	2.0	0.50	0.10	
Type 310 SS	Bal.	20.5	25.0	-	2.0	1.50	0.25	
Type 321 SS	Bal.	10.5	18.0	-	2.0	1.00	0.08	0.40 Ti
Incoloy 800	Bal.	32.5	21.0	-	1.5	1.00	0.10	0.38 Al, 0.38 Ti
9Cr-2Mo	Bal.	-	9.5	2.1	0.9	0.33	0.09	

[a] wt %

TABLE XIII. Experimental Conditions

Run No.	Bed Condition	Fluidizing Gas
1	Fully Sulfated Dolomite	5% O_2, 200 ppm SO_2, Balance N_2
2	Fully Sulfated Dolomite, 1.5 g Solid NaCl Introduced every 4h	5% O_2, 200 ppm SO_2, Balance N_2
3	Dolomite Treated with NaCl (3.0 mole % NaCl)	5% O_2, 3200 ppm SO_2, Balance N_2
4	Limestone Treated with $CaCl_2$ (0.1 mole % $CaCl_2$)	5% O_2, 3200 ppm SO_2, Balance N_2
5	Dolomite Treated with NaCl (1.0 mole % NaCl)	5% O_2, 3200 ppm SO_2, Balance N_2

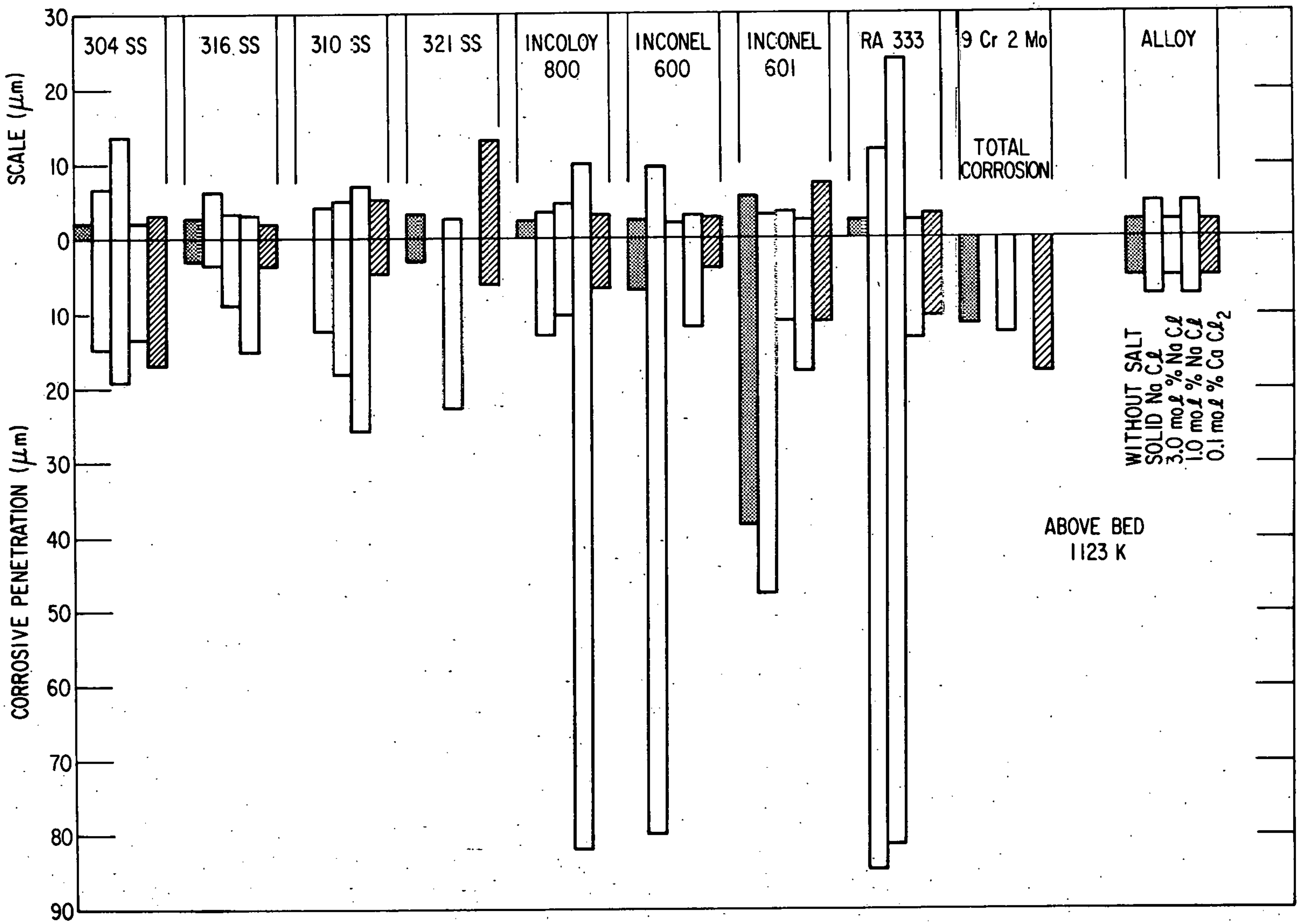

Fig. 15. Average Thickness of Surface Scale and Corrosive Penetration for Corrosion Coupons Inside the Bed for 100 h at 1123 K. ANL Neg. No. 306-78-785.

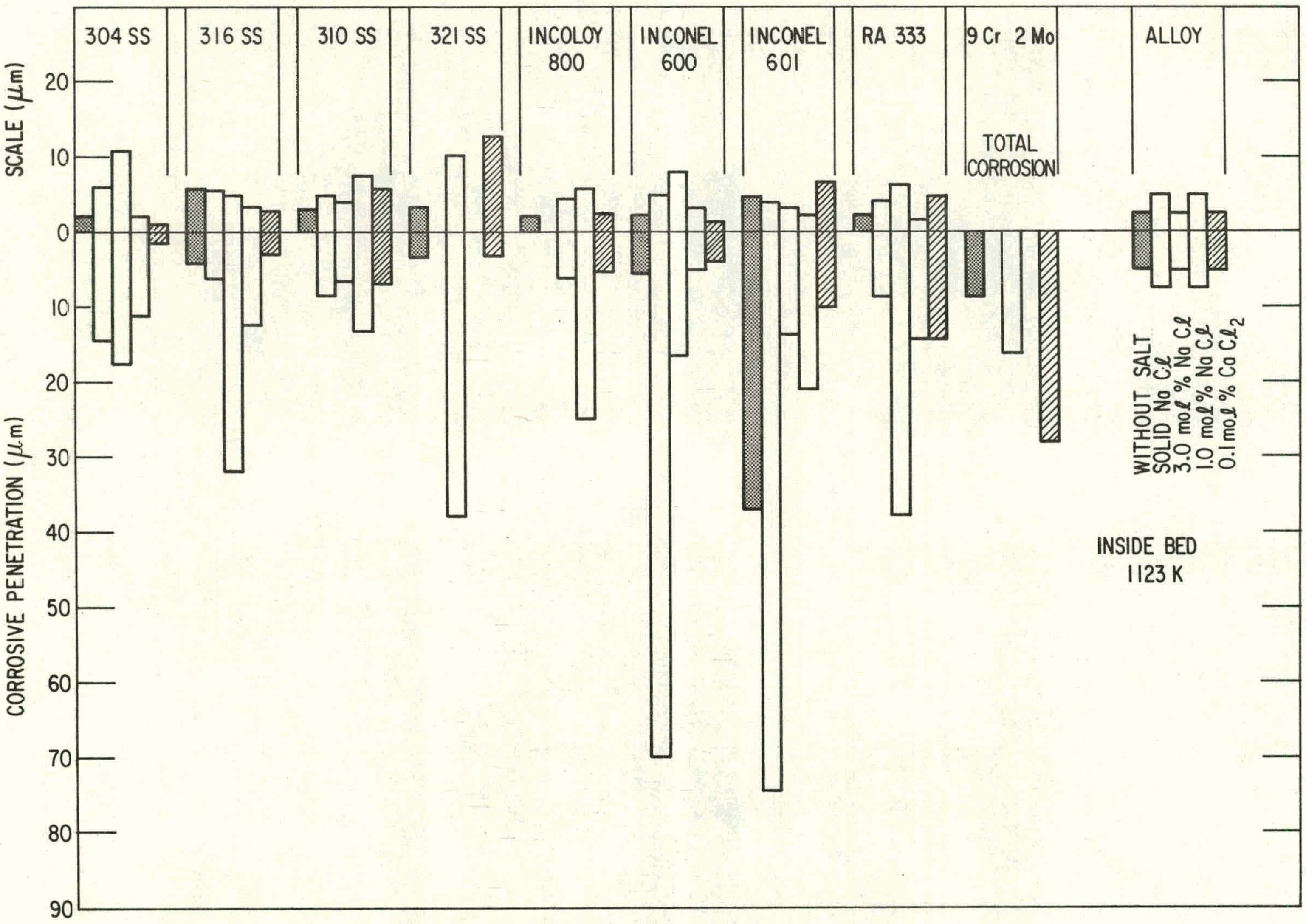

Fig. 16. Average Thickness of Surface Scale and Corrosive Penetration for Corrosion Coupons Exposed Above the Bed for 100 h at 1123 K. ANL Neg. No. 306-78-786.

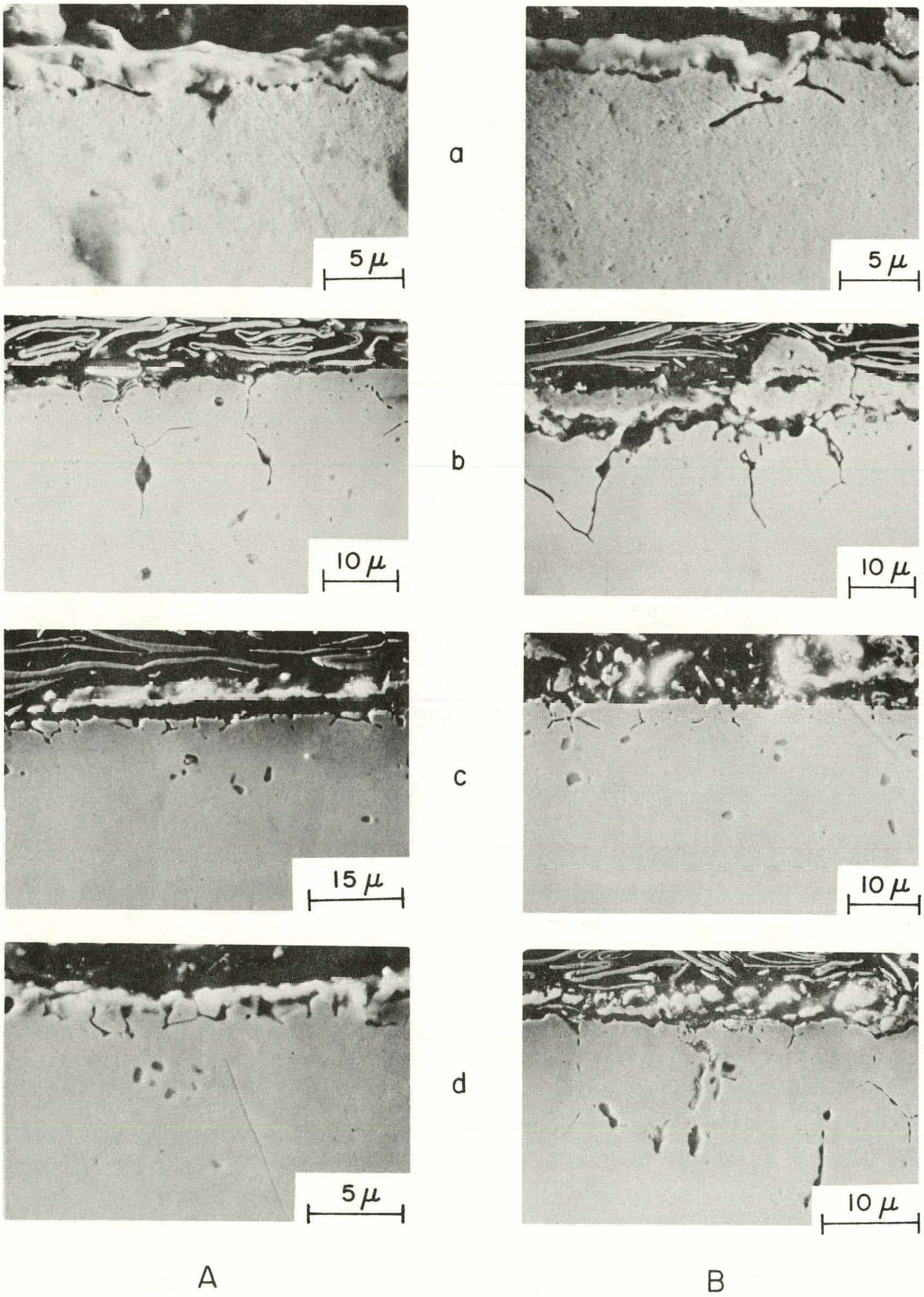

Fig. 17. SEM Micrographs of Type 304 Stainless Steel After a 100-h Exposure at 1123 K. (A) Exposed in bed, (B) exposed above bed, (a) without salt, (b) solid NaCl, (c) 1.0 mole % NaCl, and (d) 0.1 mole % $CaCl_2$. ANL Neg. No. 306-78-795.

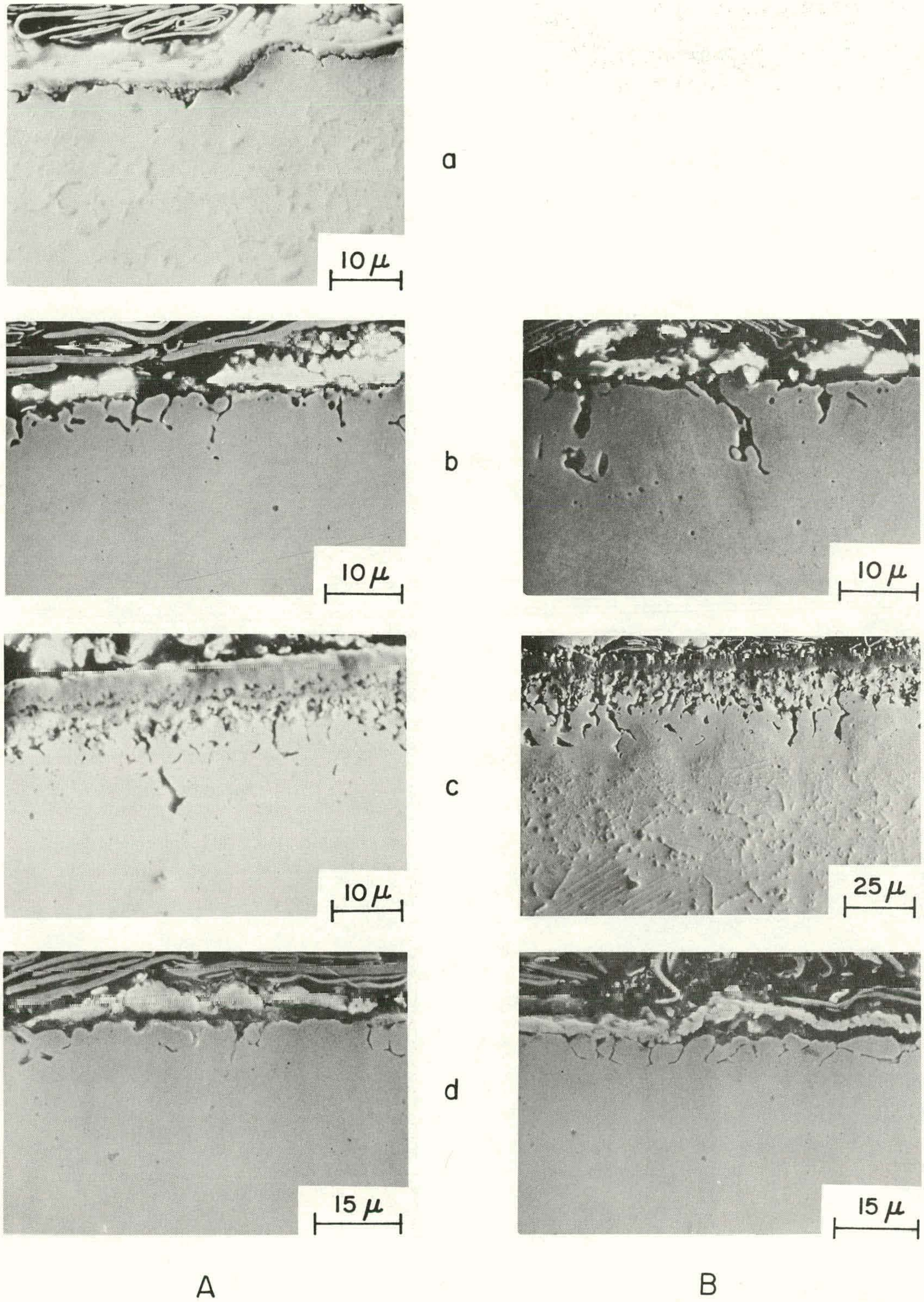

Fig. 18. SEM Micrographs of Type 310 Stainless Steel after a 100-h Exposure at 1123 K. (A) Exposed in bed, (B) exposed above bed, (a) without salt, (b) solid NaCl, (c) 1.0 mole % NaCl, and (d) 0.1 mole % $CaCl_2$. ANL Neg. No. 306-78-797.

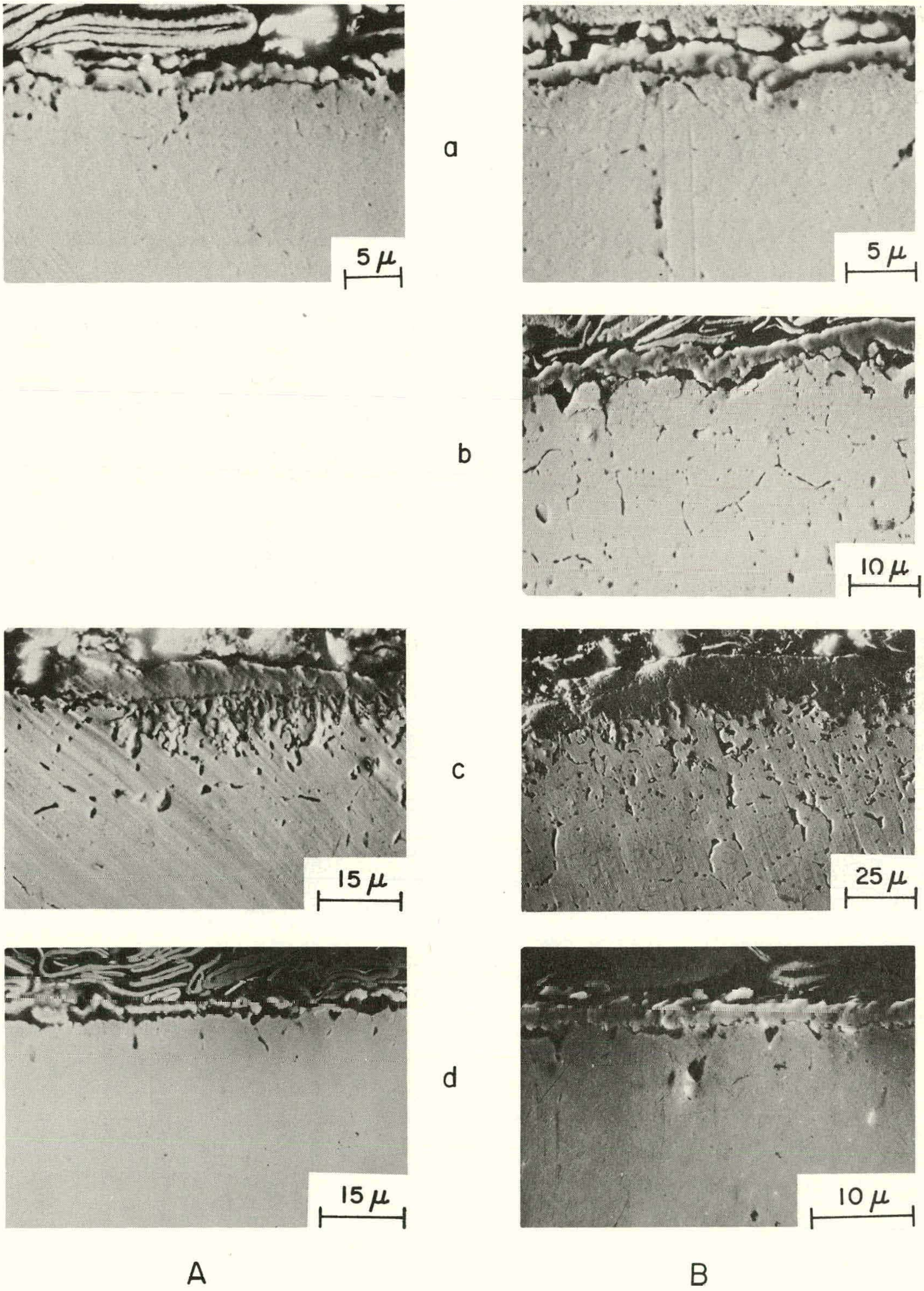

Fig. 19. SEM Micrographs of Incoloy 800 after a 100-h Exposure at 1123 K. (A) Exposed in bed, (B) exposed above bed, (a) without salt, (b) solid NaCl, (c) 1.0 mole % NaCl, and (d) 0.1 mole % $CaCl_2$. ANL Neg. No. 306-78-798.

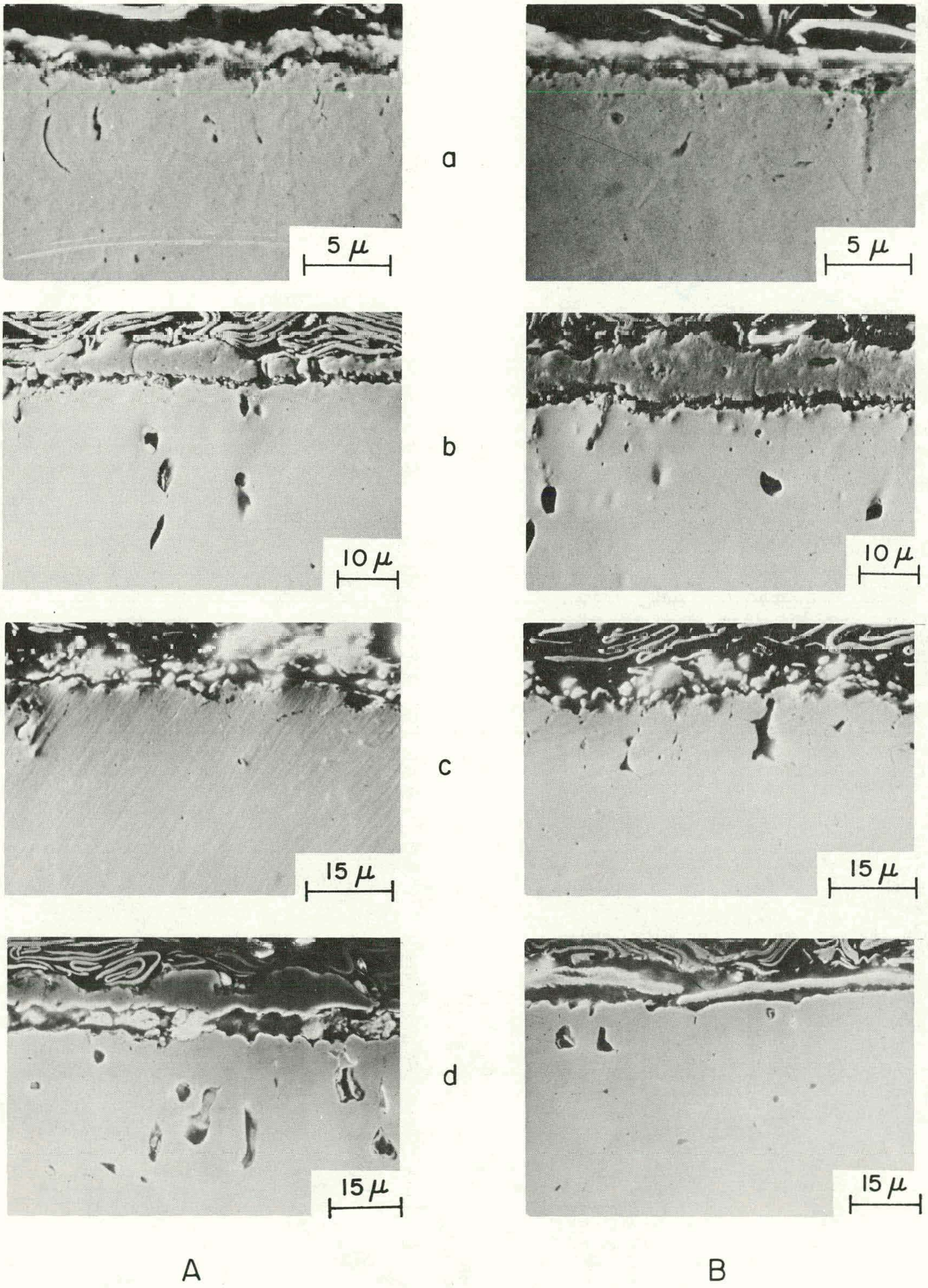

Fig. 20. SEM Micrographs of Inconel 600 after a 100-h Exposure at 1123 K. (A) Exposed in bed, (B) exposed above bed, (a) without salt, (b) solid NaCl, (c) 1.0 mole % NaCl, and (d) 0.1 mole % $CaCl_2$. ANL Neg. No. 306-78-796.

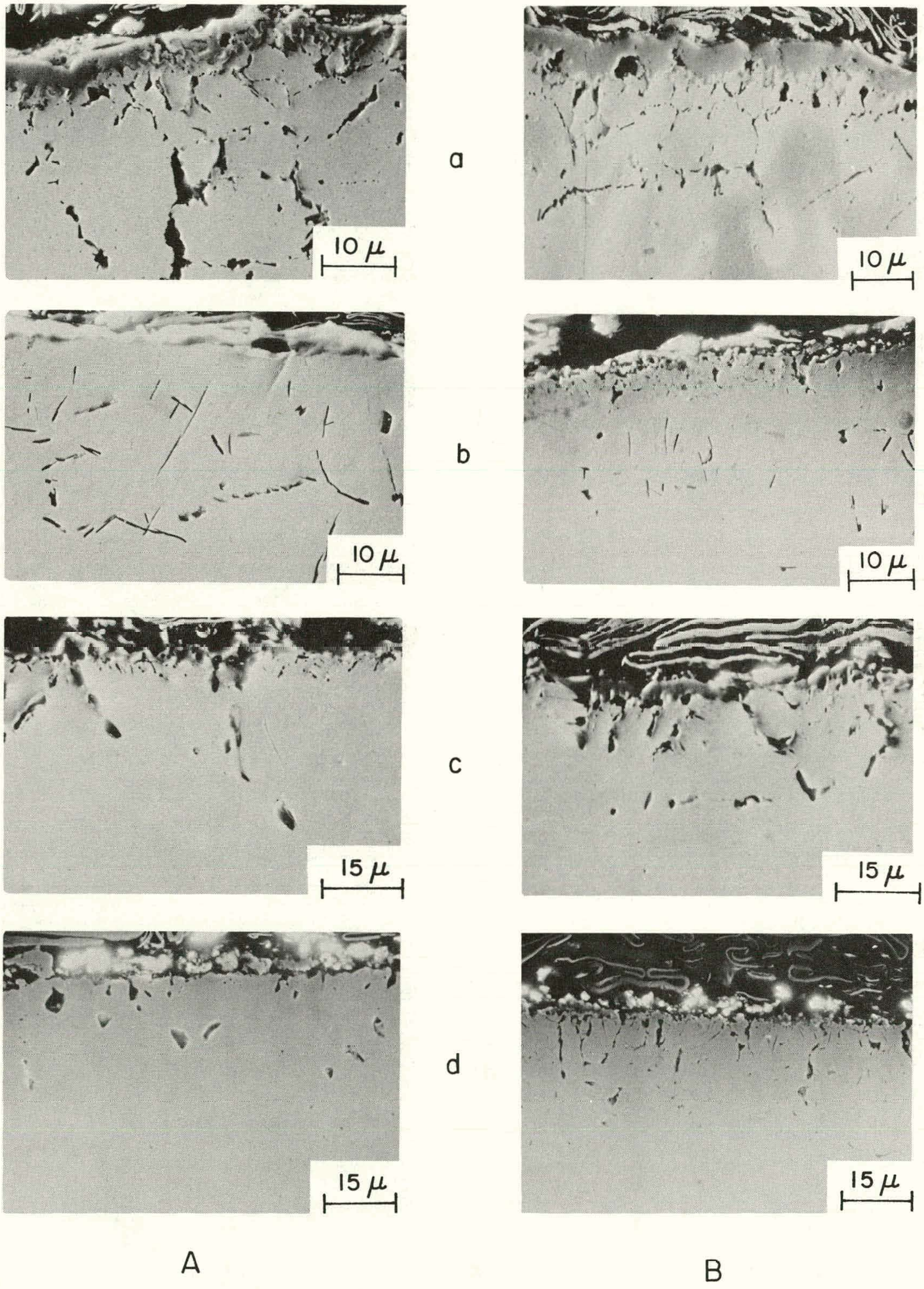

Fig. 21. SEM Micrographs of Inconel 601 after a 100-h Exposure at 1123 K. (A) Exposed in bed, (B) exposed above bed, (a) without salt, (b) solid NaCl, (c) 1.0 mole % NaCl, and (d) 0.1 mole % $CaCl_2$. ANL Neg. No. 306-78-794.

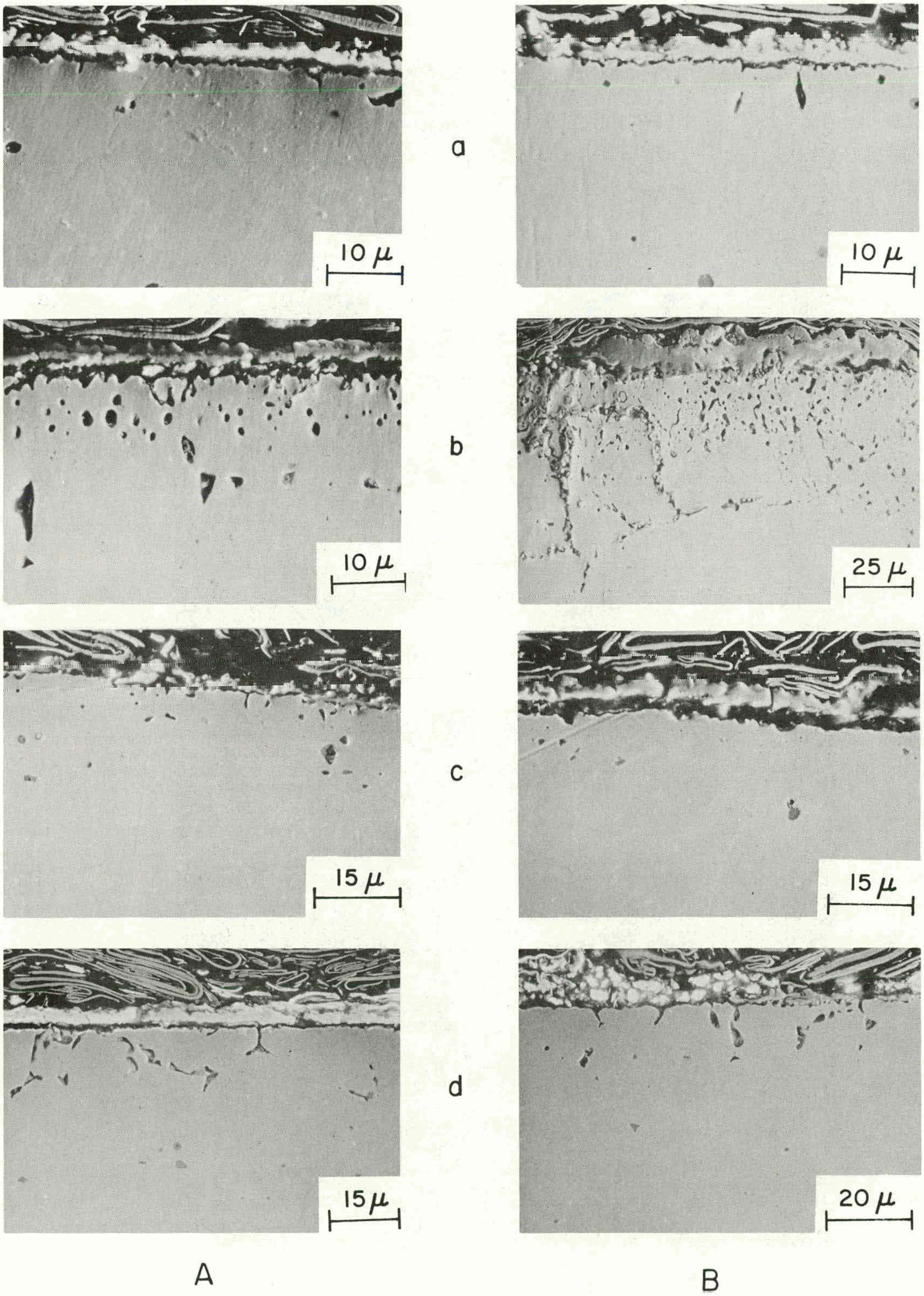

Fig. 22. SEM Micrographs of RA333 After a 100-h Exposure at 1123 K. (A) Exposed in bed, (B) exposed above bed, (a) without salt, (b) solid NaCl, (c) 1.0 mole % NaCl, and (d) 0.1 mole % $CaCl_2$. ANL Neg. No. 306-78-793.

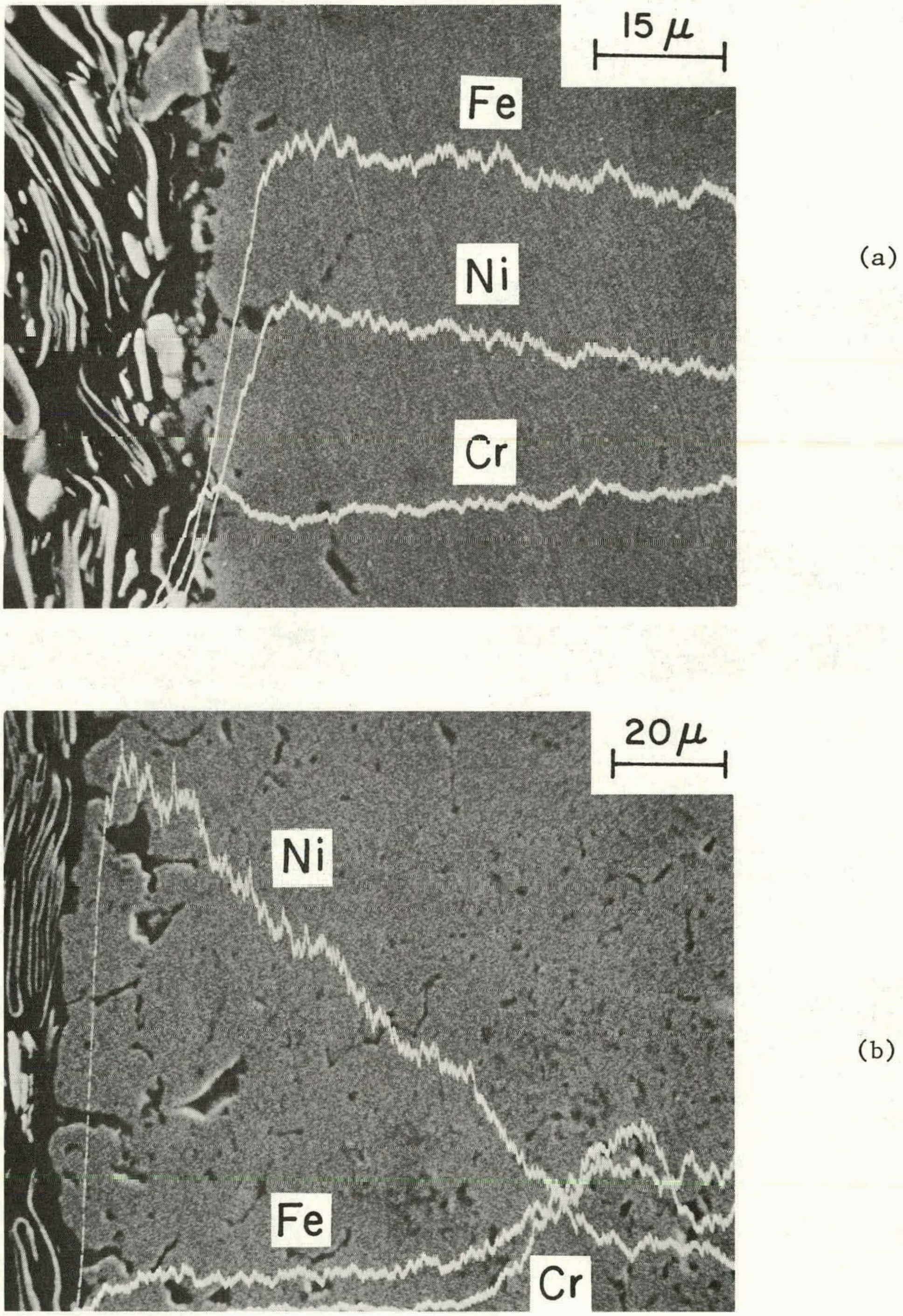

Fig. 23. X-ray Microprobe Line Analyses for Ni, Fe, and Cr on Incoloy 800 Specimens Exposed above the Bed for 100 h at 1123 K. (a) Exposure without salt and (b) with solid NaCl. ANL Neg. No. 306-78-787.

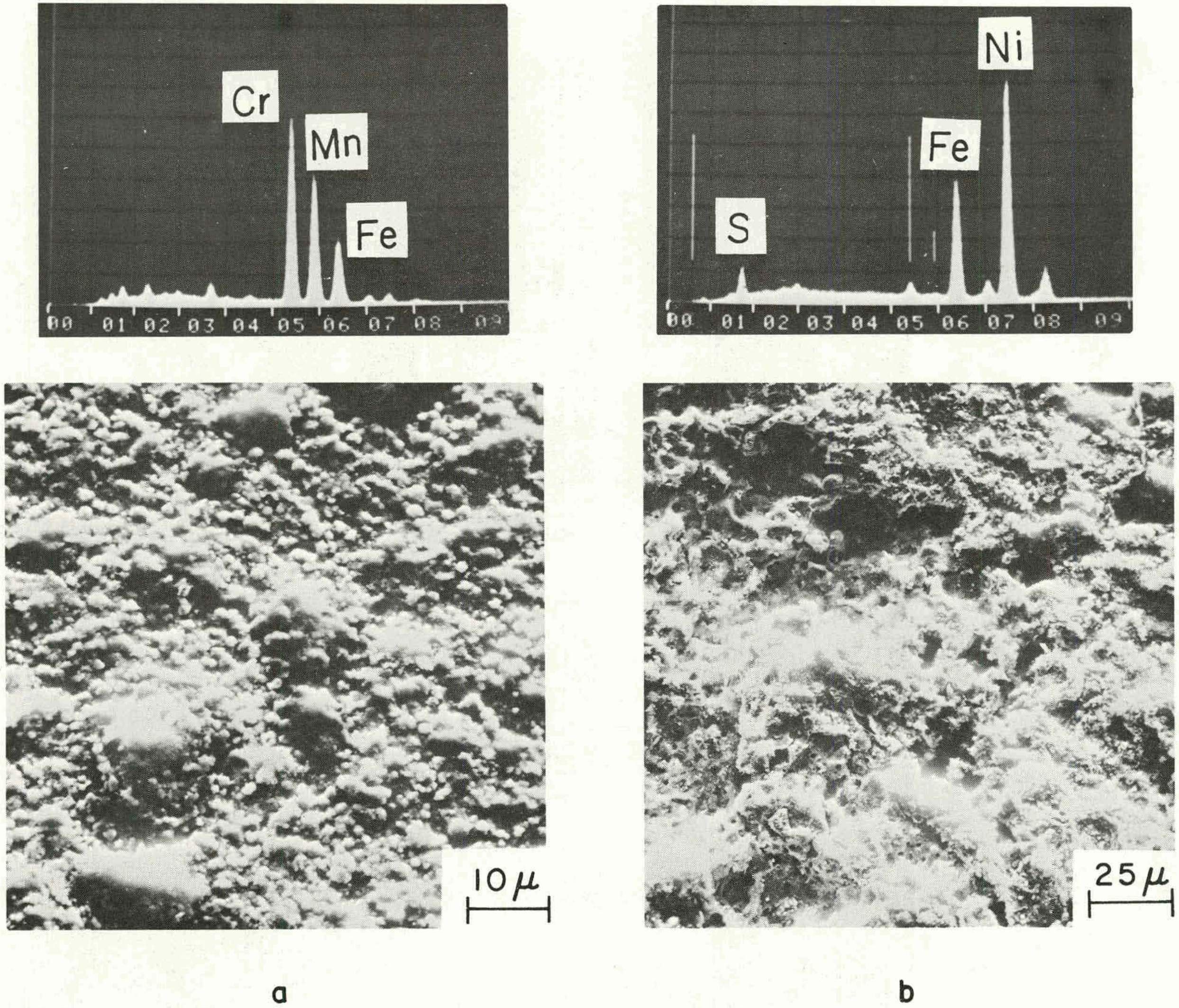

Fig. 24. SEM Micrographs and EDAX Analysis of the Surface Scales Developed on Incoloy 800 Exposed above the Bed for 100 h at 1123 K. (a) Exposure without salt and (b) with solid NaCl. ANL Neg. No. 306-78-458.

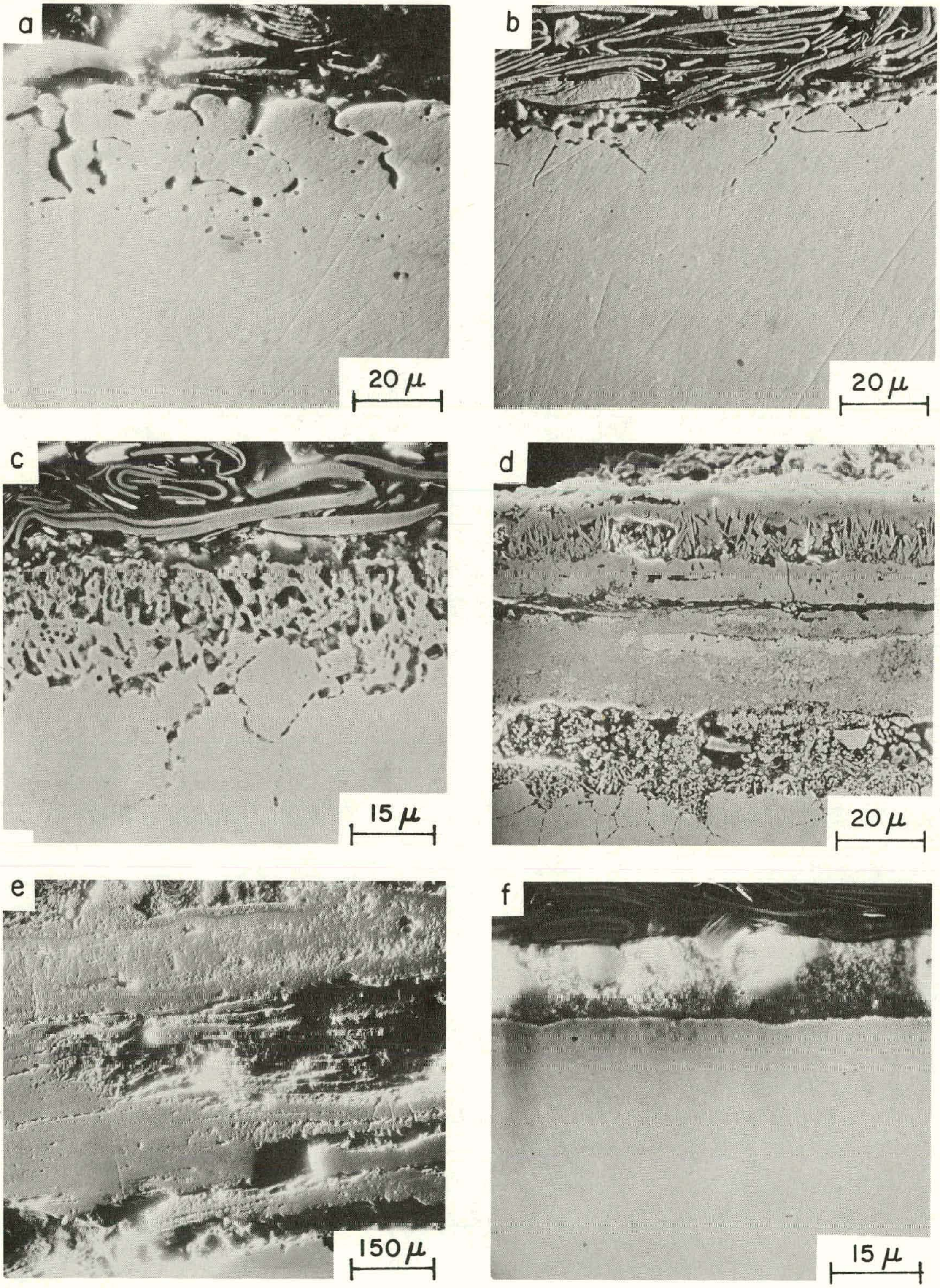

Fig. 25. SEM Micrographs of Type 304 Stainless Steel after a 100-h Exposure. (a) Exposed in bed at 1123 K, (b-f) exposed above bed at (b) 1123 K, (c) 1073 K, (d) 923 K, (e) 823 K, and (f) 723 K. ANL Neg. No. 306-78-791.

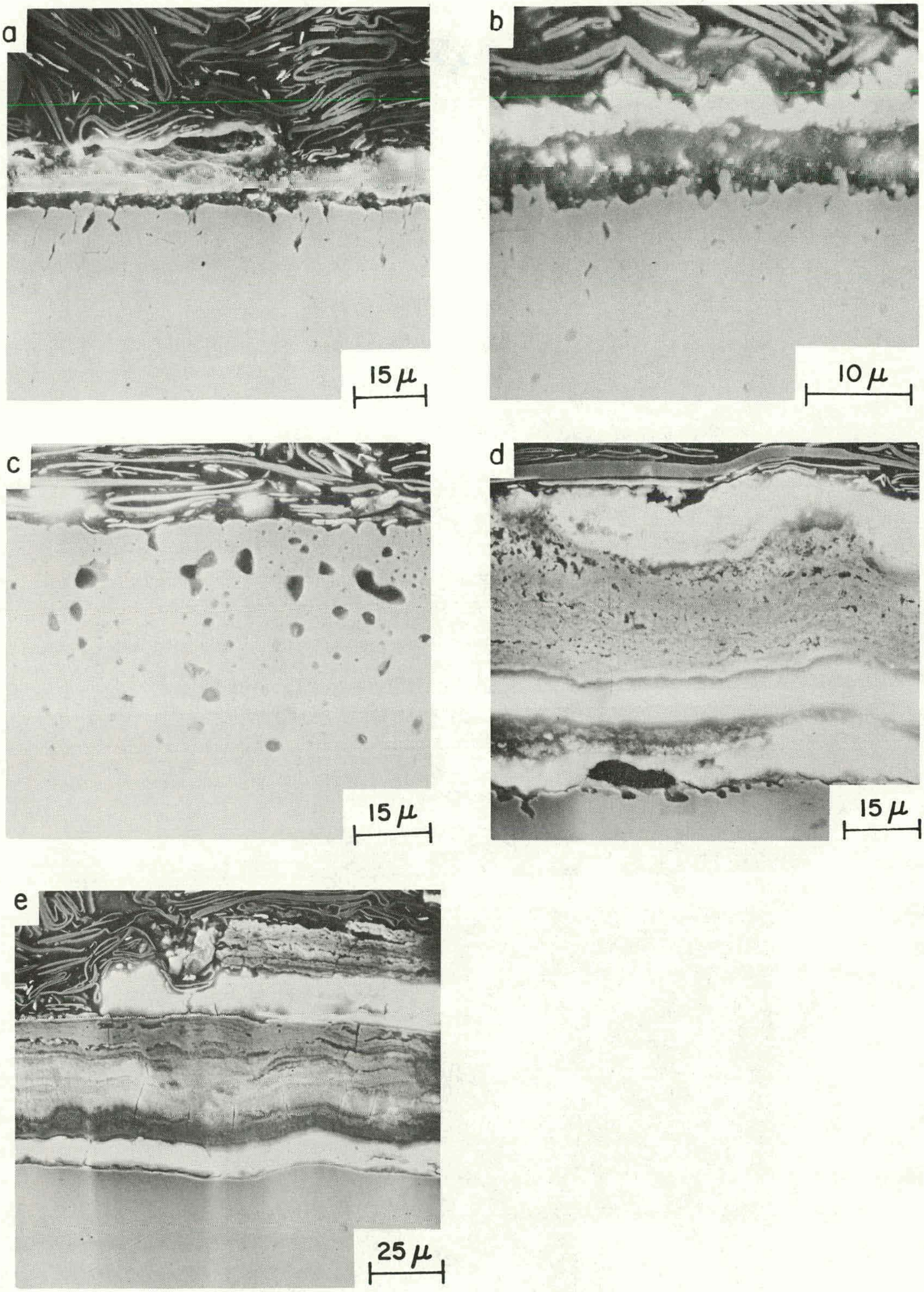

Fig. 26. SEM Micrographs of Type 310 Stainless Steel after a 100-h Exposure. (a) Exposed in bed at 1123 K, (b-e) exposed above bed at (b) 1123 K, (c) 1073 K, (d) 923 K, and (e) 823 K. ANL Neg. No. 306-78-792.

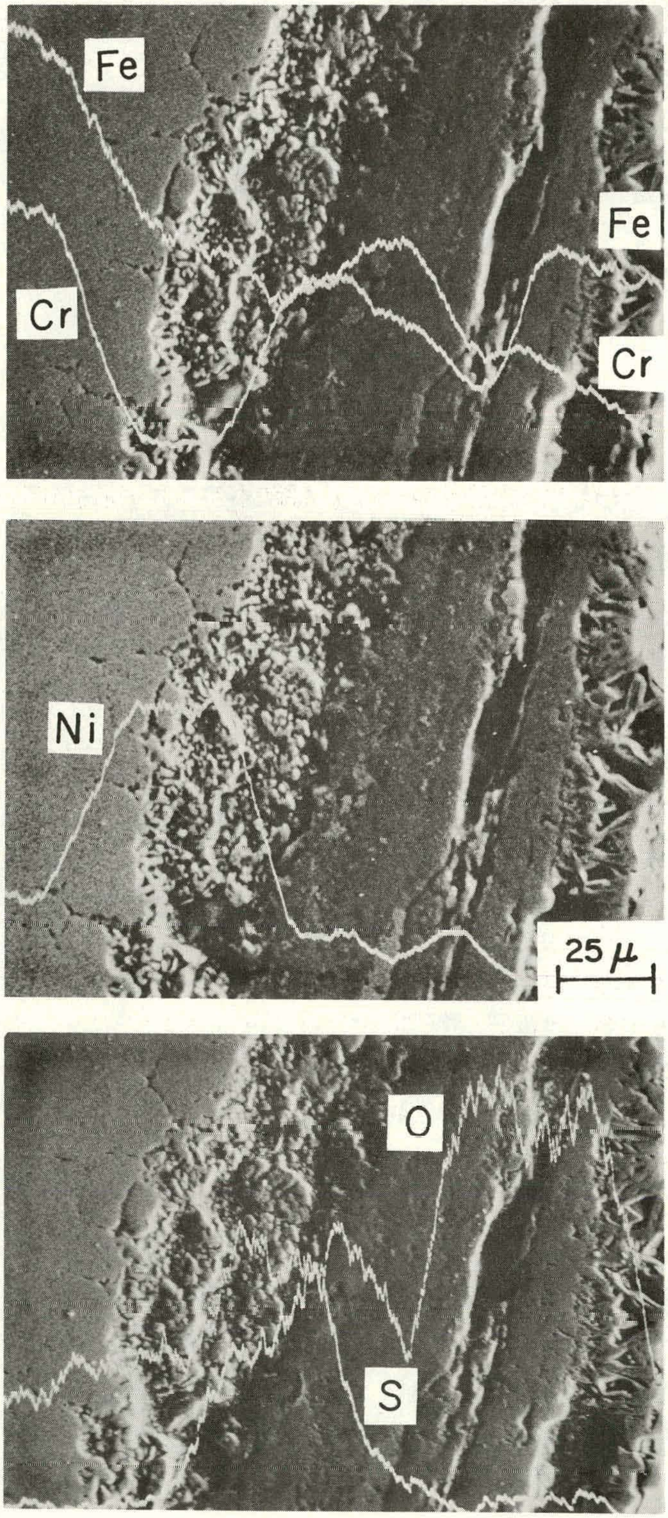

Fig. 27. X-ray Microprobe Line Analyses for Fe, Cr, Ni, O, and S on Type 304 Stainless Steel Specimen Exposed above the Bed for 100 h at 923 K. ANL Neg. No. 306-78-788.

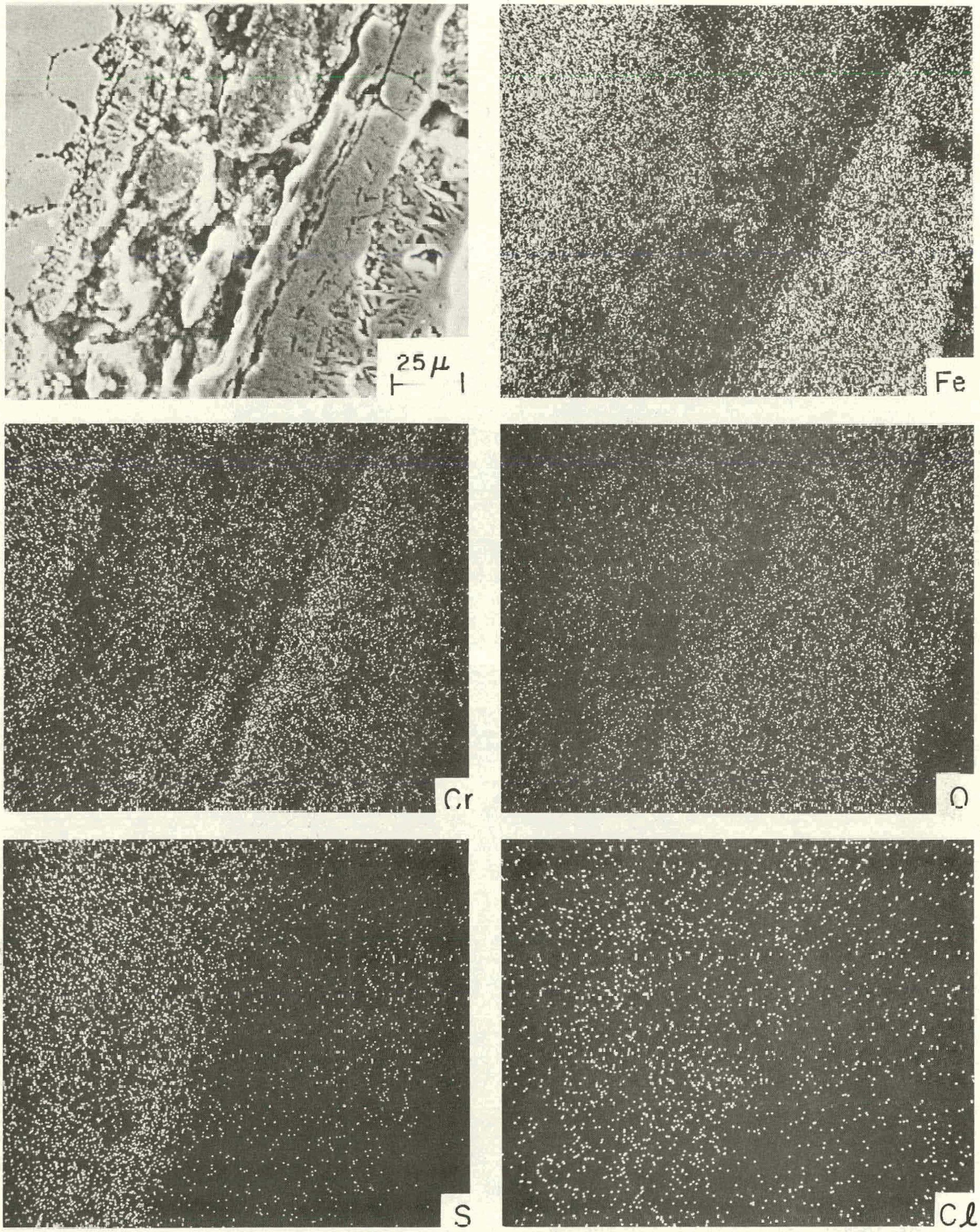

Fig. 28. SEM Micrograph and X-ray Images for Fe, Cr, O, S, and Cl of Type 304 Stainless Steel Specimen Exposed above the Bed for 100 h at 923 K. ANL Neg. No. 306-78-789.

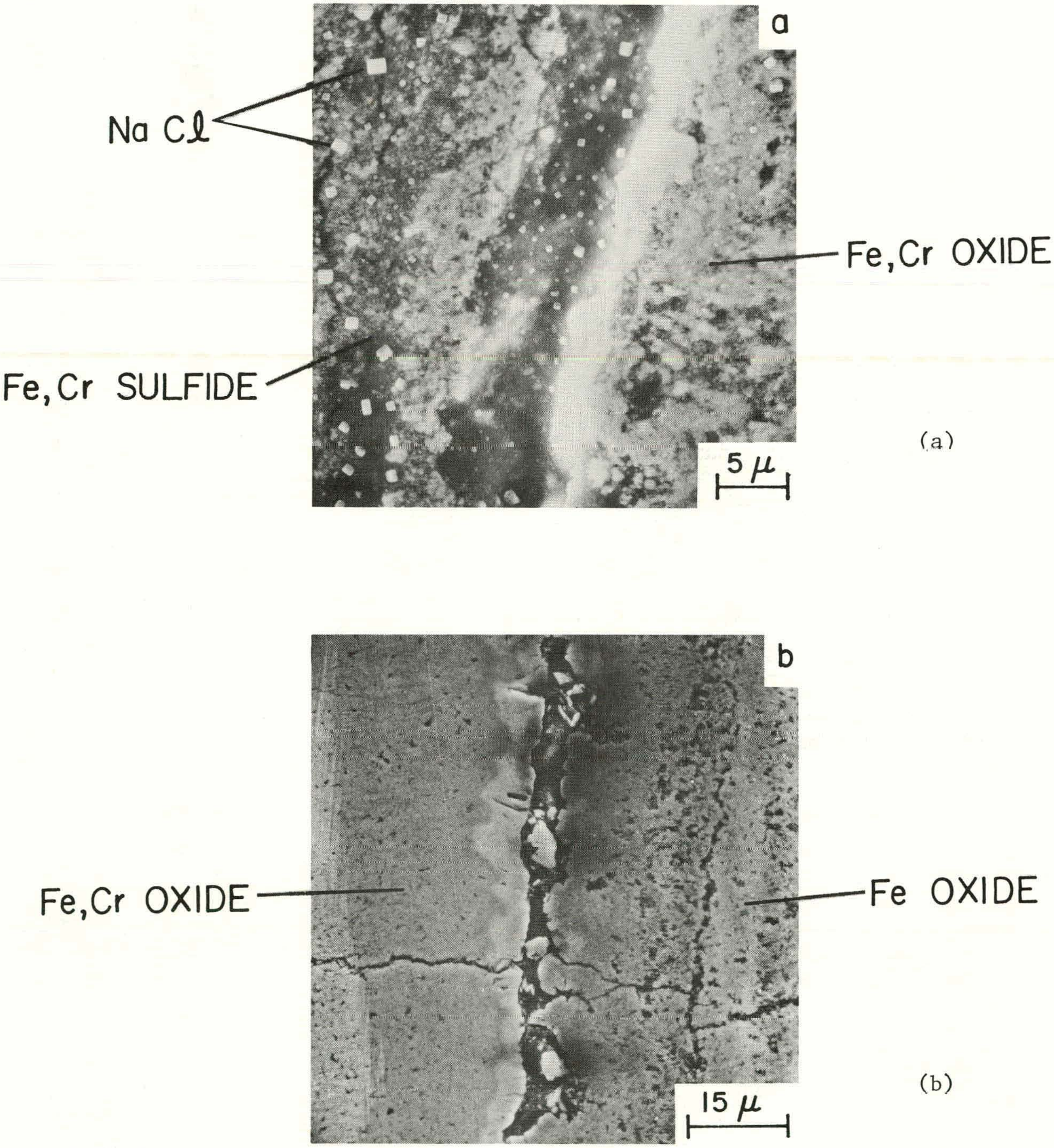

(a)

(b)

Fig. 29. SEM Micrograph of (a) Sulfide/Mixed-oxide Interface and (b) Mixed-oxide/Iron-oxide Interface Observed in Type 304 Stainless Steel Specimen Exposed above the Bed for 100 h at 823 K. ANL Neg. No. 306-78-790.

Task E -- Erosion Behavior of Materials in Coal-conversion Processes

(J.Y. Park, S. Danyluk, and W.J. Shack)

During this quarter, work has continued on the refurbishing and calibration of the high-temperature erosion-test apparatus. The particle-feeding, environmental-control and heating systems have been installed. High-temperature corrosion calibration tests will begin next quarter.

Heating and temperature control systems were checked out, and a 24-channel temperature recorder was installed. Stable temperatures up to 970°C were attained in the test chamber of the apparatus for times of over 10 hours. Calibration of flow meters for the component gas mixtures was completed. A variable-speed dc motor with speed controller was delivered and is being installed.

The test apparatus is being prepared for corrosion calibration and screening tests. The tests will be performed in an MPC-selected corrosion test atmosphere (24 H_2, 18 CO, 12 CO_2, 5 CH_4, 39 H_2O, 1 H_2S, 1 NH_3 in volume %) at atmospheric pressure and 816°C. Three separate gas mixtures (51.4 CO, 34.3 CO_2, 14.3 CH_3; 96 H_2, 4 H_2S; NH_3) and water will be fed into the test chamber at a total flow rate of 16 ml/s (2 cfh). Twelve corrosion test specimens have been prepared from Type 304 stainless steel, SAE 1015 carbon steel, Incoloy 800 and Stellite 6B for the initial calibration tests. The results of these calibration tests will be compared with data obtained in Task D and from other sources.

Task F -- Component Performance and Failure Analysis *(S. Danyluk, G.M. Dragel, C.A. Youngdahl and L. Pahis)*

The activity during this quarter involved examination of components from the HYGAS Ash Agglomerating Gasifier (AAG) and Liquid Phase Methanation (LPM) Plant. Follow-up analyses were also conducted on the failures described in the previous quarterly report. A summary of the work accomplished in the present quarter is given below.

(1) The LPM plant at HYGAS was damaged by fire in June. Two block valves that were suspected to have contributed to the cause of the fire were pressure tested in our laboratory. It was found that the valves could not sustain the specified 4.1 MPa (600 psi). These results were reported to Mr. C. Nicholson (DOE) and will be included in his final report. Since the fire also affected HYGAS piping, several pipe sections were examined metallographically to make certain that the microstructure of the piping was not adversely affected. The microstructure of the tubing that had been exposed to the fire was no different from that of unexposed piping.

(2) A visit was made to HYGAS to examine cracks in the reactor cover plate. The cracks are shallow and shavings that include these cracks are presently being analyzed.

(3) HYGAS offgas piping has been analyzed. Leaking cracks were found near welds. A weld-neck flange and a 4-in.-OD pipe have been examined to date, and the results are as follows: The leaking cracks were intergranular, and occurred ∿ 1 cm from the weld fusion line. Transgranular cracks were also found near the welds; these were not throughwall and occurred at random positions relative to the weld fusion line. Both types of cracks initiated at the ID. Figure 30 shows the morphology of typical cracks found in the weld-neck flange. The weld-prep areas were most likely the initiation sites for the intergranular cracks.

(4) Work has started on preparing thermowells of Haynes Alloy 188 for exposure to the AAG environment. Corrosion and erosion will be monitored after controlled exposures.

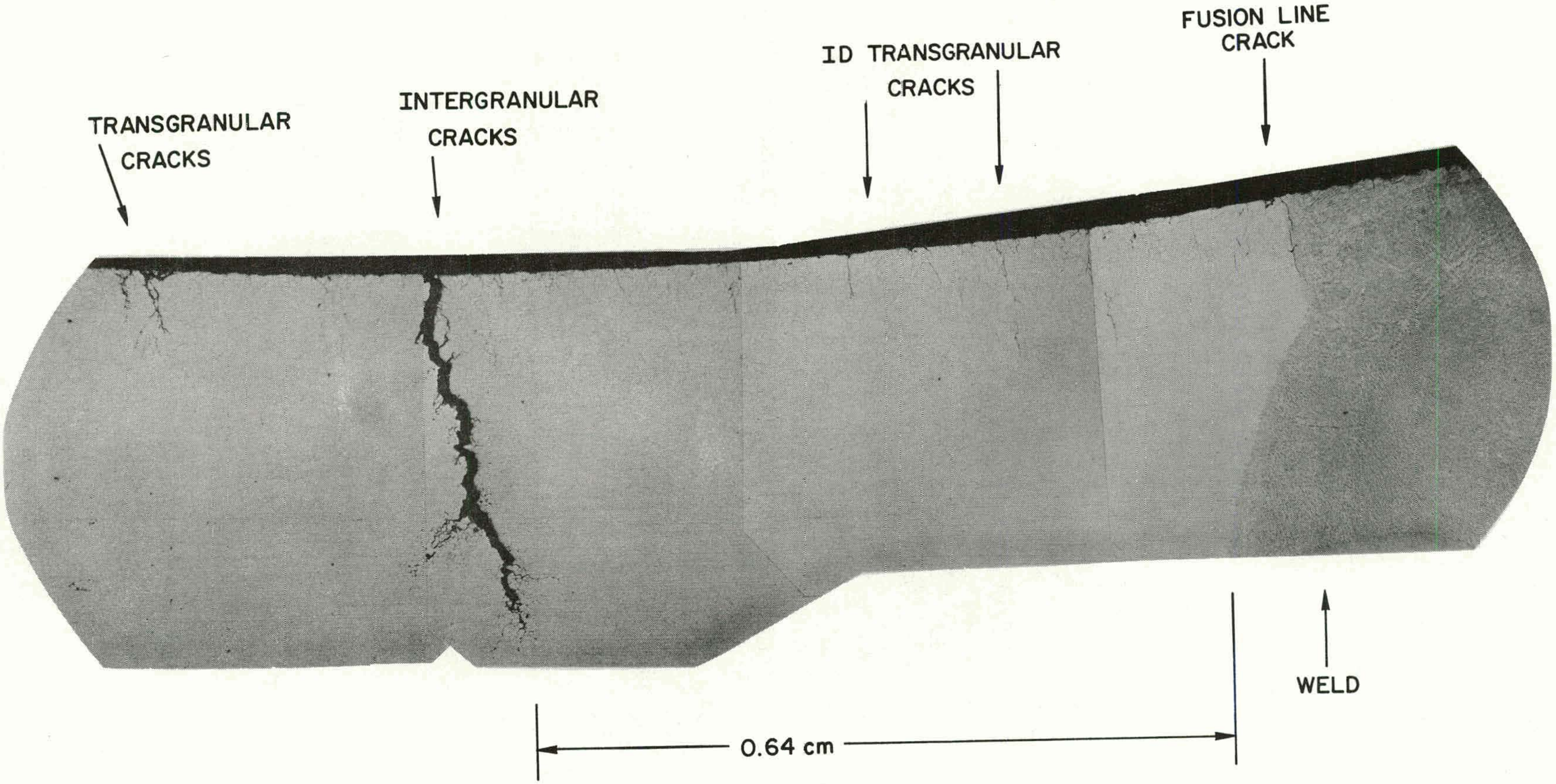

Fig. 30. Micrograph of the ID Surface of the Weld-neck Flange. The intergranular crack shown is 0.64 cm from the weld fusion line. ANL Neg. No. 306-78-928.

REFERENCES

1. Materials Technology for Coal-conversion Processes, Fourteenth Quarterly Report, April-June 1978, Argonne National Laboratory, ANL-78-79.

2. Materials Technology for Coal-conversion Processes, Thirteenth Quarterly Report, January-March 1978, Argonne National Laboratory, ANL-78-54.

3. A.B. Wood, *A Textbook of Sound,* 1930; or see 3rd Ed., 1955 (G. Bell and Sons, Ltd., London,)pp. 51-53.

4. E.H.F. Date, "Elastic Properties of Steels", J. Iron Steel Inst. *207*, 988-991 (July 1969).

5. *Properties for LMFBR Safety Analysis*, Argonne National Laboratory, ANL-CEN-RSD-76-1, Suppl. 1 (1976).

6. C. Arthur Youngdahl and William A. Ellingson, "Development of Ultrasonic Techniques for Remote Monitoring of Erosive Wear in Coal-conversion Systems," *1978 Ultrasonics Symposium Proceedings*, IEEE Cat. #78CH1344-1SU, 1978.

7. Materials Technology for Coal-conversion Processes, Twelfth Report, July-December 1977, Argonne National Laboratory, ANL-78-6.

8. Materials Science Division Coal Technology Ninth Quarterly Report, October-December 1976, Argonne National Laboratory, ANL-77-5.

Distribution for ANL-79-2

Internal:

- E. G. Pewitt
- R. G. Matlock
- B. R. T. Frost
- R. W. Weeks (6)
- N. M. O'Fallon
- O. K. Chopra
- S. Danyluk
- E. L. Stefanski
- W. A. Ellingson (6)
- J. Fischer
- K. J. Reimann
- C. A. Youngdahl
- A. A. Jonke
- T. F. Kassner
- C. R. Kennedy
- K. Natesan
- E. L. Hartig
- J. Y. Park
- R. B. Poeppel
- W. J. Shack
- A. B. Krisciunas
- ANL Contract Copy
- ANL Libraries (5)
- TIS Files (6)

External:

- DOE-TIC, for distribution per UC-90c (299)
- Manager, Chicago Operations Office
- Chief, Office of Patent Counsel, CH
- President, Argonne Universities Association
- Materials Science Division Review Committee:
  - E. A. Aitken, General Electric Co., Sunnyvale
  - G. S. Ansell, Rensselaer Polytechnic Inst.
  - R. W. Balluffi, Massachusetts Inst. Technology
  - R. J. Birgeneau, Massachusetts Inst. Technology
  - S. L. Cooper, Univ. Wisconsin
  - C. Laird, Univ. Pennsylvania
  - M. T. Simnad, General Atomic
  - C. T. Tomizuka, U. Arizona
  - A. R. C. Westwood, Martin Marietta Laboratories
- R. R. Adams, Battelle Columbus Laboratories
- E. M. Anderson, The Babcock & Wilcox Company
- W. G. Bair, Inst. of Gas Technology
- W. Bakker, Div. Systems Engineering, USDOE
- G. B. Brenneman, Maxon Corp., Muncie, Ind.
- J. A. Brooks, Amoco Oil Co., Naperville, Ill.
- M. Crowley, Standard Oil of Indiana, Naperville, Ill.
- S. J. Dapkunas, Div. Systems Engineering, USDOE
- J. Flagg, Universal Oil Products Co., Des Plaines, Ill.
- E. Fox, Stearns-Roger Corp., Homer City, Pa.
- H. E. Frankel, Div. Systems Engineering, USDOE
- S. M. Gaitonde, Commonwealth Edison Co., Maywood, Ill.
- D. Glaser, Stearns-Roger Corp., Denver
- H. Heysteck, Tuscaloosa Metallurgy Research Center, University, Ala.
- V. Hill, IIT Research Inst.
- D. Hull, Phillips Petroleum Co., Homer City, Pa.
- R. I. Jaffee, Electric Power Research Institute
- D. L. Keairns, Westinghouse Research Labs.
- H. Leavenworth, Albany Metallurgy Research Center
- A. V. Levey, Lawrence Berkeley Laboratory
- R. Lewis, Synthane Pilot Plant, USDOE/FE, Pittsburgh
- G. Long, Northern Illinois Gas Co., Aurora
- R. M. Lundberg, Commonwealth Edison Co., Chicago
- M. M. Mamoun, Inst. Gas Technology, Chicago
- J. M. O'Donnell, The Lummus Co., Bloomfield, N.J.
- A. L. Plumley, Combustion Engineering Power Systems, Windsor

J. Pope, Science Applications, Inc.
F. A. Prange, Phillips Petroleum Corp., Bartlesville
A. Sagüés, Kentucky Center for Energy, Lexington
A. Schaeffer, Metals Properties Council, New York
S. J. Schneider, National Bureau of Standards (2)
J. R. Schorr, Battelle Columbus Laboratories
G. Sorrell, Exxon Research and Engineering Co., Florham Park
J. Stevenson, Rolla Metallurgy Research Center
J. Sudbury, Consolidated Coal Co., Library, Pa.
C. Whitten, Peabody Coal Co., Columbia, Tenn.